

Detection of the YORP Effect for Small Asteroids in the Karin Cluster

V. Carruba^{1,2}, D. Nesvorný², D. Vokrouhlický³

(1) *UNESP, Univ. Estadual Paulista, Grupo de Dinâmica Orbital e Planetologia,
Guaratinguetá, SP, 12516-410, Brazil*

(2) *Department of Space Studies, Southwest Research Institute, Boulder, CO, 80302, USA*

(3) *Institute of Astronomy, Charles University, V Holešovičkách 2, Prague, CZ-18000,
Czech Republic*

ABSTRACT

The Karin cluster is a young asteroid family thought to have formed only $\simeq 5.75$ My ago. The young age can be demonstrated by numerically integrating the orbits of Karin cluster members backward in time and showing the convergence of the perihelion and nodal longitudes (as well as other orbital elements). Previous work has pointed out that the convergence is not ideal if the backward integration only accounts for the gravitational perturbations from the Solar System planets. It improves when the thermal radiation force known as the Yarkovsky effect is accounted for. This argument can be used to estimate the spin obliquities of the Karin cluster members. Here we take advantage of the fast growing membership of the Karin cluster and show that the obliquity distribution of diameter $D \simeq 1\text{--}2$ km Karin asteroids is bimodal, as expected if the YORP effect acted to move obliquities toward the extreme values (0° or 180°). The measured magnitude of the effect is consistent with the standard YORP model. The surface thermal conductivity is inferred to be $0.07\text{--}0.2 \text{ W m}^{-1} \text{ K}^{-1}$ (thermal inertia $\simeq 300\text{--}500 \text{ J m}^{-2} \text{ K}^{-1} \text{ s}^{-1/2}$). We find that the strength of the YORP effect is roughly $\simeq 0.7$ of the nominal strength obtained for a collection of random Gaussian spheroids. These results are consistent with a surface composed of rough, rocky regolith. The obliquity values predicted here for 480 members of the Karin cluster can be validated by the light-curve inversion method.

1. Introduction

The Karin family with the estimated age of 5.75 ± 0.05 My is one of the youngest families in the main belt (Nesvorný et al. 2002; Nesvorný & Bottke 2004). Because of its recent

formation, it is possible to numerically integrate the orbits backward in time and demonstrate the young age by showing that the orbits of individual members converge together at the time of the parent body breakup. Improving on previous work, Nesvorný & Bottke (2004) have shown that a precise reconstruction of the orbital histories requires that the Yarkovsky effect is taken into account in the backward integration. This allowed them to infer the semi-major axis drift rate for individual members of the Karin cluster and verify, for the first time, how the Yarkovsky effect operates on the main belt asteroids over million-year-long timescales. A by-product of this study was a determination of spin obliquities for 70 individual members of the Karin cluster with absolute magnitudes $H < 16$ (roughly diameters $D > 2$ km for albedo $p_V = 0.2$).

Many new asteroids have been discovered since the last dynamical analysis of the Karin cluster. Here we repeat the analysis of Nesvorný & Bottke (2004) with an orbital catalog that contains nearly seven times more asteroids than what was available back in 2004. In Sect. 2, we revise the Karin family membership by applying the usual clustering method on the new orbital catalog. The taxonomical and albedo interlopers are eliminated. We then apply a more stringent criterion of the Karin family membership by requiring that orbits converge to each other $\simeq 5.75$ My ago. In Sect. 3, we use the method developed in Nesvorný & Bottke (2004) to estimate the Yarkovsky drift rates of individual bodies. This data is compared to the theoretical expectations for the Yarkovsky effect.

We find that the distribution of spin obliquities ε of small Karin members ($D \simeq 1\text{--}2$ km) is bimodal with only very few values near $\varepsilon = 90^\circ$ and peaks for smaller and larger obliquities (Sect. 4). It is shown that this obliquity distribution is consistent with an initially random orientation of spin axes that was modified by the YORP effect (Sects. 5-7; e.g. Rubincam 2000, Čapek & Vokrouhlický 2004). In Sect. 8, we apply a standard YORP model to estimate the thermal conductivity and calibrate the strength of the YORP effect. The results are discussed in Sect. 9. Finally, we perform new numerical simulations with the Yarkovsky force and/or gravitational perturbations of (1) Ceres (Sect. 10), and discuss the latter as a stochastic factor that sets firm limits on what can be achieved with this type of study. Section 11 presents our conclusions.

2. Family identification

To define the Karin cluster membership, we first turned our attention to the family identification data from Nesvorný et al. (2015). In that work, the Karin cluster was identified using the Hierarchical Clustering Method (HCM hereafter), and a velocity cut-off of 10 m s^{-1} in the domain of the proper orbital elements $(a, e, \sin i)$ (see Table 2 in

Nesvorný et al. 2015, for further details). To eliminate possible interlopers, we adopted the classification scheme of DeMeo & Carry (2013). Specifically, we used the fourth release of the Sloan Digital Sky Survey-Moving Object Catalog (SDSS-MOC4; Ivezić et al. 2001), and computed the *gri* slope and $z' - i'$ colors. In addition, we used information from three major photometric/spectroscopic surveys: the Eight-Color Asteroid Survey (ECAS; Zellner et al. 1985; Tholen 1989), Small Main Belt Spectroscopic Survey (SMASS; Xu et al. 1995; Bus & Binzel 2002a,b), and Small Solar System Objects Spectroscopic Survey (S3OS2; Lazzaro et al. 2004). There were 13 objects with known taxonomical information in total, six of which have a C-complex taxonomy and are therefore incompatible with the S-type taxonomy of the Karin cluster. After eliminating these objects we end up with a sample of 535 Karin family members.

To account for possible members of the Karin cluster that may have been excluded by the velocity cutoff used in Nesvorný et al. (2015), we define a box in proper $(a, e, \sin i)$ space with the following ranges: 2.855 to 2.878 au in a , 0 to 0.1 in e , and 0.0122 to 0.0611 in $\sin i$. These values correspond to the full range of $(a, e, \sin i)$ values in the Karin cluster from Nesvorný et al. (2015), plus a margin of 0.002 au in a , and 0.03 in e and $\sin i$. After eliminating SDSS-MOC4 interlopers, we were left with a sample of 1117 additional objects. Of these, only 8 objects have known albedo values $p_V < 0.1$ (Masiero et al. 2012), and can be potential albedo interlopers.

We proceed by computing the components (v_r, v_t, v_W) the terminal ejection velocity V_{ej} from the Gauss equations (e.g., Murray & Dermott 1999)

$$\begin{aligned} \frac{\delta a}{a} &= \frac{2}{na(1-e^2)^{1/2}} [(1+e\cos f)\delta v_t + (e\sin f)\delta v_r], \\ \delta e &= \frac{(1-e^2)^{1/2}}{na} \left[\frac{e+\cos f+e\cos^2 f}{1+e\cos f} \delta v_t + \sin f \delta v_r \right], \\ \delta i &= \frac{(1-e^2)^{1/2}}{na} \frac{\cos(\omega+f)}{1+e\cos f} \delta v_W. \end{aligned} \quad (1)$$

where $\delta a = a - a_{\text{ref}}$, $\delta e = e - e_{\text{ref}}$ and $\delta i = i - i_{\text{ref}}$ with a_{ref} , e_{ref} and i_{ref} being a reference value, and f and ω are the true anomaly and perihelion argument of the disrupted parent body at the time of the breakup. Here we used $f = 30^\circ$ and $f + \omega = 50.5^\circ$ (Nesvorný & Bottke 2004).

We find that the HCM members of the Karin family have $V_{ej} < 70 \text{ m s}^{-1}$. As a final membership filter we therefore include bodies in the extended set with $V_{ej} < 80 \text{ m s}^{-1}$ (i.e., with a 10 m s^{-1} buffer). In total, 489 asteroids in the Karin family and 189 in an extended family pass this filter. A plot of the orbital distribution of 480 Karin family members, after applying additional criteria discussed in the following text, is shown in Fig. 1.

To reconstruct the past orbital history of Karin cluster members, we numerically integrated the orbits of all $489 + 189 = 678$ potential members with the symplectic integrator known as *SWIFT_MVSF* (Levison & Duncan 1994), modified by Brož (1999) to include the online filtering of the osculating elements. The integration included the gravitational effects of all Solar System planets (the radiation forces were ignored). The initial velocity vectors of asteroids and planets were multiplied by -1 such that, effectively, the orbits are tracked back into the past. The normal orbital longitudes Ω and ϖ were recovered from this simulation by using relationships

$$\begin{aligned}\Omega &= \Omega^* + 180^\circ, \\ \varpi &= \Omega^* - \omega^*,\end{aligned}\tag{2}$$

where Ω^* and ω^* are the nodal longitude and perihelion argument computed from the backward integration with *SWIFT_MVSF*. The integration time step was set to be 1 day.

Figure 2 shows the result of our backward simulation. We plot there $\Delta\Omega = \Omega - \Omega_{\text{Karin}}$ and $\Delta\varpi = \varpi - \varpi_{\text{Karin}}$, where Ω_{Karin} and ϖ_{Karin} are the orbital longitudes of (832) Karin. Note that the angles converge in Fig. 2 in the time interval between -5.6 and -5.8 My, which is a clear evidence that the Karin cluster formed at that time (see also Novaković et al. (2012) for details on the method of convergence of orbital angles as a membership criteria). From the 678 member candidates identified above we found that 576 objects have angles converging with $\Delta\Omega < 60^\circ$ and $\Delta\varpi < 60^\circ$ at $-5.8 < t < -5.6$ My. These 576 objects represent our final membership list. Relative to Nesvorný & Bottke (2004) we identified 479 new members of the Karin cluster.

3. Measurement of the Yarkovsky Drift

The convergence of angles in Fig. 2 is not ideal because our numerical integration only accounted for the gravitational effects of planets and ignored all else. In reality, the orbits of small members of the Karin cluster are affected by the Yarkovsky effect that arises as a recoil force from a directional emission of the thermal radiation (e.g., Bottke et al. 2006). The main orbital effect of the Yarkovsky force is to either decrease or increase the semi-major axis of an orbit. Since the precession frequency of angles Ω and ϖ depends on the semi-major axis, the Yarkovsky effect is thus expected to influence the convergence of Ω and ϖ . This dependence can be used to determine the Yarkovsky drift rates for individual members of the Karin cluster (Nesvorný & Bottke 2004).

According to Nesvorný & Bottke (2004), the values of $\Delta\Omega_j$ and $\Delta\varpi_j$ for asteroid j at

time $t = -(\tau + \Delta t)$ are:

$$\Delta\Omega_j(t) = -\frac{1}{2}\frac{\partial s}{\partial a}(\delta a_j - \delta a_1)\tau - (s_j - s_1)\Delta t, \quad (3)$$

$$\Delta\varpi_j(t) = -\frac{1}{2}\frac{\partial g}{\partial a}(\delta a_j - \delta a_1)\tau - (g_j - g_1)\Delta t, \quad (4)$$

where τ is the estimated family age, Δt is a small correction and δa_j is the total semi-major axis drift over time τ . Here we neglected the initial spread of these angles produced by V_{ej} , which should be of the order of 1° (Nesvorný & Bottke 2004). Index $j = 1$ refers to (832) Karin. Quantities $\partial s/\partial a$ and $\partial g/\partial a$ define how the nodal and apsidal precession frequencies change with a . Here we adopt $\partial s/\partial a_P = -70.0 \text{ arcsec yr}^{-1} \text{ au}^{-1}$ and $\partial g/\partial a_P = 94.4 \text{ arcsec yr}^{-1} \text{ au}^{-1}$ (Nesvorný & Bottke 2004). Corrections $(s_j - s_1)\Delta t$ and $(g_j - g_1)\Delta t$ vanish when $\Delta t = 0$. See Nesvorný & Bottke (2004) for further discussion of Eqs. (3) and (4).

By solving these two equations we can obtain the values of $\Delta a_j = \delta a_j - \delta a_1$ required to compensate for $\Delta\Omega$ and $\Delta\varpi$ obtained from our backward integration at time t . In general, for an arbitrary time t , the two determinations of Δa_j from $\Delta\Omega$ and $\Delta\varpi$ will be different. As the time t approaches the correct age of the family, the difference is expected to disappear. We use this method to determine the best estimate of τ . Specifically, we define a χ^2 -like variable of the form

$$\chi(t) = \sum_{j=2}^N \frac{|\Delta a_j^\Omega - \Delta a_j^\varpi|}{(N-1)}, \quad (5)$$

where Δa_j^Ω and Δa_j^ϖ are the two determinations at time t , and search for the minimum of $\chi(t)$. When applied to the $N = 576$ previously identified members of the Karin cluster, we found that the minimum occurs for $\tau = 5.746 \pm 0.011 \text{ My}$. This result is in an excellent agreement with the age estimate of Nesvorný & Bottke (2004) who found $\tau = 5.75 \pm 0.05 \text{ My}$. The higher accuracy of our estimate is justified by the fact that our sample of the Karin cluster members is $\simeq 7$ times larger than that of Nesvorný & Bottke (2004).

How well the semi-major axis drift rates determined here compare with those from Nesvorný & Bottke (2004)? To answer this question we computed the mean value $\Delta a_j = (\Delta a_j^\Omega + \Delta a_j^\varpi)/2$ for each individual member and compared these results with those obtained in Nesvorný & Bottke (2004). Figure 3 shows the result of this comparison. There is a very good correlation between the drift values obtained back in 2004 and here. Unfortunately, Nesvorný & Bottke (2004) explicitly listed the Δa_j values obtained for $t = -5.7$ and -5.8 My , but not for the time corresponding to the best age estimate. To use these estimates in Fig. 3, we have computed the mean of these values. Since the drift rates obtained for these times are systematically higher than the ones for $t = -5.75 \text{ My}$, the mean is also slightly

higher. This explains why in Fig. 3 the estimates for $t = -5.75$ My obtained in our work are systematically higher, by about $\simeq 20\%$, than the values inferred from the 2004 work.

Figure 4 shows the Δa_j values obtained here for the Karin cluster members, including hundreds of small members that were not known previously. As in Nesvorný & Bottke (2004), we eliminated from the original sample of 576 members all objects with orbital uncertainties in semi-major axis larger than 10^{-4} au, and those whose incompatibly large differences between Δa_j^Ω and Δa_j^ϖ would suggest that they are probably interlopers (namely those with $|\Delta a_j^\Omega - \Delta a_j^\varpi| > 1.5 \times 10^{-4}$ au, a value significantly larger than that for the vast majority of the studied possible Karin member). The latter criterion eliminated only two objects.

The results shown in Fig. 4 are in excellent agreement with Fig. 3 in Nesvorný & Bottke (2004). The measured magnitude of the semi-major axis drift increases with H , as expected for the Yarkovsky effect, whose strength is inversely proportional to the object diameter. The Yarkovsky drift magnitude over the estimated age of the family nearly reaches $\simeq 10^{-3}$ au for the smallest members, which is just the right value for $D \simeq 1\text{--}2$ km asteroids with extreme values of obliquities (see below and Bottke et al. 2006, for more discussion).

4. The Bi-modality of Drift Rates

The small members in Fig. 4 ($H \geq 16\text{--}16.5$) appear to have a bimodal distribution of the semi-major axis drifts with either relatively large positive or large negative values. This trend is reminiscent of the semi-major axis distribution found in several older asteroid families, where the distribution of the semi-major axis values is similarly bimodal. This trend has been interpreted as a result of the interplay between the Yarkovsky and YORP effects (see, e.g., Vokrouhlický et al. 2006a, 2015; Nesvorný et al. 2015). A similar line of reasoning suggests that Karin cluster is at the initial stage of this process.

Specifically, we suggest that the YORP effect acted on the Karin cluster members to slightly shift their obliquities toward extreme values (0° and 180°), and this affected the overall magnitude of the accumulated Yarkovsky drifts. Obviously, the Δa values measured in Section 2 are relatively small ($< 10^{-3}$ au; Fig. 4), and the Yarkovsky effect has not altered the overall structure of the Karin family in proper element space. Instead, the small change of the semi-major axes has only influenced the convergence of angles (as we discussed in the previous section). Before we present a detailed model of the Yarkovsky and YORP effects in Sect. 8, here we verify whether the measured magnitude of drifts is in agreement with our theoretical expectations for the Yarkovsky effect.

First, in Fig. 5, we divide the accumulated drifts Δa_j by the family age τ , obtaining the effective drift rate $\langle da/dt \rangle_j = \Delta a_j / \tau$ for each Karin member. A distinct characteristic of the Yarkovsky effect is that the drift rate is inversely proportional to body's diameter D . Therefore, in Fig. 5, we also plot isolines of $1/D = \text{const}$ (gray lines). The highlighted gray lines correspond to a drift value $\pm 1.4 \times 10^{-4}$ au My $^{-1}$ for a $D = 1.4$ -km body. These isolines approximately envelope the distribution of measured $\langle da/dt \rangle$.

This trend has been noticed previously (Nesvorný & Bottke 2004), but here we also characterize the distribution for $D = 1 - 2$ km asteroids which were not known in 2004. Presumably, the Karin members with the $\langle da/dt \rangle$ values close to the enveloping lines have an extreme value of the obliquity, because the Yarkovsky effect is maximized for $\varepsilon = 0^\circ$ or $\varepsilon = 180^\circ$. Asteroids with the $\langle da/dt \rangle$ values inside the zone bracketed by the enveloping lines should have intermediate values of the obliquity. Various complications of this simple interpretation arise because the semi-major axis drift rate due to the Yarkovsky effect depends on other parameters as well (such as, e.g., the asteroid rotation period). Bodies with the same obliquity value can thus drift at (slightly) different speeds (see the next section).

5. Maximum Drift Rates

Here we compare the measured maximum drift rates ($\langle da/dt \rangle \simeq 1.4 \times 10^{-4}$ au My $^{-1}$ for $D = 1.4$ km) with the Yarkovsky effect theory developed in Vokrouhlický (1999) (see also Vokrouhlický et al. 2015). Assuming a large body limit (i.e., penetration depth of the diurnal thermal wave much smaller than the body size) and keeping just the diurnal variant of the Yarkovsky effect, we have

$$\frac{da}{dt} \simeq \frac{4\alpha}{9} \frac{\Phi}{n} \frac{\Theta}{1 + \Theta + \frac{1}{2}\Theta^2} \cos \varepsilon, \quad (6)$$

where $\alpha = 1 - A$, with A being the Bond albedo, $\Phi = (\pi D^2 F)/(4mc)$, $F \simeq 166.4$ W m $^{-2}$ is the solar radiation flux at the mean heliocentric distance of the Karin cluster, m is the asteroid mass, c is the velocity of light, and n is the orbital frequency.

Note that $\Phi \propto 1/D$ which provides the aforementioned proportionality of the Yarkovsky effects with $1/D$. The thermal parameter $\Theta = \Gamma \sqrt{\omega}/(\epsilon \sigma T_\star^3)$ depends on the surface thermal inertia Γ , rotation frequency ω , and surface infrared emissivity ϵ , the Stefan-Boltzmann constant σ and sub-solar temperature $T_\star = [\alpha F/(\epsilon \sigma)]^{1/4}$.

While we could use the thermal inertia Γ as an independent parameter, we follow the tradition of the Yarkovsky effect studies and express it as $\Gamma = \sqrt{K \rho_s C}$, where K is the surface thermal conductivity, ρ_s is the surface density and C the surface thermal capacity.

For the sake of definiteness we fix $\rho_s = 2 \text{ g cm}^{-3}$ and $C = 680 \text{ J/kg/K}$, and consider the thermal conductivity K to be a free parameter (instead of Γ). The relationship $da/dt \propto \cos \varepsilon$ gives the dependence of the Yarkovsky effect on obliquity. Obviously, the maximum drift rates will occur for $\varepsilon = 0^\circ$ (maximum positive rate) and $\varepsilon = 180^\circ$ (maximum negative rate).

We now use Eq. (6) to compute the values da/dt that would be expected for the $D = 1.4 \text{ km}$ Karin members. For definiteness, we assume $A = 0.1$, $\epsilon = 0.9$, and bulk density $\rho_b = 2.5 \text{ g cm}^{-3}$. The rotation rate ω and thermal conductivity K are varied within a reasonable range of values. The maximum drift rate of the Yarkovsky effect is obtained with $\varepsilon = 0^\circ$. Figure 6 shows the results. To illustrate things we chose two typical values of the rotation period: 6 hr (solid line) and 18 hr (dashed line). The gray trapezoid in Fig. 6 is where the maximum drift rates are similar to the maximum drift rates inferred from small members of the Karin cluster ($(1.3 - 1.4) \times 10^{-4} \text{ au My}^{-1}$).

We note that the maximum $\langle da/dt \rangle$ values inferred from the small Karin cluster members are fully reasonable. In fact, they are somewhat smaller than the optimal Yarkovsky drift rate for $D = 1.4 \text{ km}$ Karin members that could be as large as $\simeq 2.2 \times 10^{-4} \text{ au My}^{-1}$ (for low surface thermal inertia). The measured values of $(1.3 - 1.4) \times 10^{-4} \text{ au My}^{-1}$ (Fig. 5) can be used to constrain the thermal conductivity/inertia. Assuming the typical rotation periods between 3 and 24 hr, the measured value correspond the surface thermal conductivity in the range $0.02 - 0.2 \text{ W m}^{-1}\text{K}^{-1}$ (Fig. 6). This translates to the thermal inertia values $\simeq (170 - 500) \text{ J m}^{-2}\text{K}^{-1}\text{s}^{-1/2}$. These results are consistent with the determination of the thermal inertia for small near-Earth asteroids (e.g., Delbò et al. 2007, and M. Delbò updates, personal communication).

6. Prograde vs. Retrograde Rotators

We now collect the $\langle da/dt \rangle$ measurements in the two highlighted size intervals shown in Fig. 5: (i) interval I1 with $D = 0.9 - 1.7 \text{ km}$, and (ii) interval I2 with $D = 2.5 - 3.5 \text{ km}$. The former contains 280 measurements, while the latter contains 55 measurements. The primary data-set that we use here to analyze the YORP effect is I1. The set I2 is a control case that we use to make sure that our model (see below) consistently fits data for large sizes as well (note that I2 was roughly the size range available in Nesvorný & Bottke (2004)).

Figure 7 shows the distribution of Δa values in the zones I1 (top) and I2 (bottom). In I1, there are 139 and 141 data points with negative and positive values of Δa , respectively. Recalling that this reflects the sign of $\cos \varepsilon$ (see Eq. 6), we therefore find that an approximately equal number of small Karin cluster members has prograde and retrograde rotation.

This is interesting: the measurement of the drift rate for larger members indicates that there are more retrograde rotators among the largest fragments. For example, the six members with $D > 4$ km, except for (832) Karin itself, are inferred to have a retrograde rotation (Nesvorný & Bottke 2004). (832) Karin itself rotates in a prograde sense with a long rotation period (e.g., Slivan & Molnar 2012). This asymmetry, however, already disappears for the interval of sizes corresponding to I2, where there are 29 and 26 cases with negative and positive values of Δa , respectively.

The median Δa values for the negative and positive rotators in I1 are $\simeq -4.3 \times 10^{-4}$ au and $\simeq 3.4 \times 10^{-4}$ au. Thus the peak of negative values is slightly more extended than the peak of positive values. There may be a physical reason for this. Part of the difference could be caused by the neglected drift of 832 Karin itself. However, considering that the maximum drift of Karin computed using Vokrouhlický (1999) model of the Yarkovsky effect, the WISE estimated diameter, and the values of the parameters of the Yarkovsky force from Brož et al. (2013) is of the order of 6×10^{-5} au, i.e., smaller than the observed difference, other mechanisms may be at play. Recall that the obliquity evolution of the prograde rotators can be influenced by the spin-orbit resonances (e.g., Vokrouhlický et al. 2003, 2006b). If various other parameters such as the rotation period and dynamical ellipticity are favorable for capture in a resonance, the obliquity may end up oscillating around an equilibrium resonant point (e.g., Vokrouhlický et al. 2003). This may halt the usual YORP-driven obliquity evolution of prograde rotators toward the extreme values, and produce an asymmetry of the accumulated drifts (note that the retrograde rotators are not subject to resonant capture; see Fig. 27 in Vokrouhlický et al. (2006b)). A detailed investigation of the spin-orbit dynamics is left for future work.

7. Comparison with Standard YORP Theory

Here we verify whether the YORP hypothesis for the origin of the bimodal distribution in the top panel of Fig. 7 is consistent with the standard YORP theory. The strength of the YORP effect has a stronger dependence on D than the Yarkovsky effect (it scales with $\propto 1/D^2$ rather than $\propto 1/D$ of the Yarkovsky effect; e.g., Vokrouhlický et al. (2015)). This is why the Yarkovsky effect is detected in both size intervals I1 and I2, while the YORP-effect-induced bi-modality is apparent in I1 but not in I2. Assuming that the initial distribution of the spin vectors of small Karin members was isotropic, we estimate that the bimodal distribution in I1 requires a characteristic change of $\simeq 0.5$ in $\cos \varepsilon$ over the Karin cluster age. This roughly corresponds to an obliquity change of $\sim 30^\circ$ - 40° .

Čapek & Vokrouhlický (2004) modeled the YORP effect for a statistical sample of smooth Gaussian spheroids with $D = 2$ km and a heliocentric distance $a = 2.5$ au. Figure 11 in their paper shows that the maximum obliquity change of these bodies is typically 8.6° per My (the maximum change happens for $\varepsilon \simeq 35^\circ$). An average rate for an arbitrary obliquity is roughly one half of this value, or 4.3° per My, which would accumulate to $\sim 25^\circ$ over the Karin family age. The YORP strength scales as $\propto 1/(Da)^2$. Using this scaling we estimate that the obliquity of $D = 1.4$ km asteroids (characteristic size in the interval I1) should have changed, on average, by $\sim 38^\circ$. This is exactly what is required to explain the measured bi-modality in the interval I1. On the other hand, the estimated obliquity change of $D = 3$ km bodies in the interval I2 is only $\sim 8^\circ$, which is clearly too small to appreciably affect the distribution.

8. The Yarkovsky-YORP Model

Encouraged by the estimates discussed in the previous section, we now proceed by constructing a simple model for the Yarkovsky and YORP effects on small Karin cluster members. We assume that the fragments initially created in the Karin-cluster formation event had: (i) an isotropic distribution of spin axis vectors, and (ii) their rotation rates were distributed according the Maxwellian distribution (e.g., Pravec et al. 2002). Impact simulations, such as the ones in Nesvorný et al. (2006), can be used to test whether (i) is reasonable. As for (ii), we note that the Maxwellian distribution represents a good proxy for the distribution of rotation rates of fragments in the laboratory-scale impact experiments (e.g., Giblin et al. 1998).

In our simulations, we track the obliquity ε and rotation-rate ω of each of the fragments as they evolve by the YORP effect. The basic formulation of the YORP effect has been developed by Rubincam (2000). Čapek & Vokrouhlický (2004) extended this approach to also include the effects of the surface thermal conductivity, and computed the characteristic YORP strength for a large sample of smooth irregular shapes (the so-called Gaussian spheroids). Their results can be summarized as follows.

The obliquity and rotation-rate evolution is given by two differential equations

$$\frac{d\omega}{dt} = f(\varepsilon) , \quad (7)$$

$$\frac{d\varepsilon}{dt} = \frac{g(\varepsilon)}{\omega} , \quad (8)$$

where f and g are functions of obliquity. Each asteroid, having its own distinct shape, is described by different functional forms f and g , but in a statistical sense the characteristic

evolution can be obtained from the median functions derived in Čapek & Vokrouhlický (2004). In particular, we use the median values determined for the thermal conductivity $K = 0.01$ W/m/K (see their Figs. 8 and 11 in Čapek & Vokrouhlický (2004)). In this setup, the obliquities always evolve toward the extreme values $\varepsilon = 0^\circ$ and 180° , and the rotation rate may either increase or decrease when these asymptotic values are reached.

Čapek & Vokrouhlický (2004) found that the tendency toward increasing or decreasing the rotation rate is roughly the same, at least for the statistical sample of asteroid shapes they tested. This means that the value of the function f is equally likely positive or negative when $\varepsilon = 0^\circ$ or 180° . The f and g functions given in Čapek & Vokrouhlický (2004) are rescaled here to $D = 1.4$ km (corresponding to I1) using $f \propto 1/D^2$ and $g \propto 1/D^2$.

Over the past decade a number of very detailed approaches have been developed to model the YORP effect (see, e.g., Vokrouhlický et al. 2015, for a review). One of the major findings of these works was a recognition that the small-scale surface irregularities can have an important contribution to the overall YORP strength. For example, the results of Rozitis & Green (2012) and Golubov et al. (2010) indicate that the f and g functions can have a somewhat smaller magnitude than the ones obtained for a smooth surface. Additionally, a rough surface can trigger a tendency of the YORP effect to increase of the rotation rate.

We introduce two empiric parameters in our YORP model to account for these complications (see Bottke et al. (2015) for a similar approach). First, we set $f = c_{\text{YORP}} f_0$ and $g = c_{\text{YORP}} g_0$, where f_0 and g_0 are the median functions from Čapek & Vokrouhlický (2004), and c_{YORP} is a free strength parameter that expresses the actual strength of the YORP effect relative to f_0 and g_0 . As noted above, we expect that $c_{\text{YORP}} < 1$. Second, we introduce an asymmetry parameter δ_{YORP} , defined as the fraction of bodies that undergo slow down of their rotation rate ($1 - \delta_{\text{YORP}}$ is the fraction that is spun up). The original model Čapek & Vokrouhlický (2004) gives $\delta_{\text{YORP}} = 0.5$, but considering the surface roughness, values $\delta_{\text{YORP}} < 0.5$ may be more appropriate. The best fit values of parameters c_{YORP} and δ_{YORP} can be obtained from a fit to the measured distribution of obliquities.

We numerically integrate Eqs. (7) and (8) using a simple Euler-type integration scheme with a time-step of 0.01 My. The initial obliquity and rotation period values are chosen on random. Each simulation is repeated 10 times with different initial values. The simulations are stopped at $\tau = 5.746$ My, which is our best estimate of the Karin family age (Sec. 3). As the time progresses, for each individual body we accumulate the change of the semi-major axis Δa by the Yarkovsky effect from

$$\Delta a_{\text{model}} = \int_0^\tau \left(\frac{da}{dt} \right) dt = \frac{4\alpha}{9} \frac{\Phi}{n} \int_0^\tau \frac{\Theta}{1 + \Theta + \frac{1}{2}\Theta^2} \cos \varepsilon dt . \quad (9)$$

The parameters entering the right hand side of this equation were explained in Sect. 5. Note that some of the variables, assumed to be constant, were pulled in front of the integral in (9), but some other variables were left in the integrand (e.g., Θ and ε). Note that the latter parameters change due to the YORP effect. In particular, $\Theta \propto \sqrt{\omega}$. To keep things simple, in each run we use a single value of the thermal surface conductivity K for all bodies, but vary K from one run to another. The bulk density of bodies is assumed to be 2.5 g/cm^3 . Below we will discuss how the results change for different density assumptions.

Once the simulation is over, the model distribution of Δa_{model} values is compared with the measured distribution of Δa shown in Fig. 7 (top panel). Because our model is not designed to reproduce any asymmetry in the distribution of obliquities (see discussion in Sec. 3), we modify the distribution of measured drifts by folding the negative and positive bins onto each other. This leads to a symmetrical distribution shown by the red line in Fig. 9.

In each simulation, we fix δ_{YORP} and run the model for different values of c_{YORP} and K parameters. We then attempt to minimize the difference between Δa_{model} and the measured Δa distribution. We use a bin size of $1.5 \times 10^{-4} \text{ au}$ (as in Fig. 7), which leaves us with $N = 12$ bins with useful information. Our minimization procedure uses a χ^2 -like target function:

$$\chi^2 = \sum \left(\frac{n_{\text{model}} - n}{\sigma_n} \right)^2, \quad (10)$$

where the summation is performed over the 12 bins, n is the number of measurements and n_{model} the number of model bodies in each bin.

The denominator σ_n expresses the uncertainty of each n value. A common practice is to set $\sigma_n \simeq \sqrt{n}$. By adopting this assumption we find that our best-fit solutions would give $\chi^2 \simeq 13$, which is slightly larger than the number of bins. This may mean that our simple model is incomplete or slightly inaccurate. For example, as we discussed above, we do not model the effect of spin-orbit resonances that may be important for the prograde rotators. It is also possible that a better result could be obtained if two c_{YORP} parameters were used, one that multiplies the f function and one that multiplies the g function.

Instead of investigating the possible physical reasons for this slight discrepancy, which would be a considerable work on its own, here we opted for a simple fix by setting $\sigma_n \simeq \sqrt{2n}$. Our best fits give $\chi^2 \simeq 6.5$ with this definition. The confidence region in parameters (K, c_{YORP}) around the best fit solution was defined as $\chi^2 < N$, where $N = 12$.

9. The Yarkovsky-YORP model: best-fitted parameters

We found that the results only weakly depend on δ_{YORP} . The best fits were obtained $0.3 < \delta_{\text{YORP}} < 0.5$. We therefore fixed $\delta_{\text{YORP}} = 0.4$ in all subsequent simulations. Figure 8 shows the main result of these simulations. The inferred values of the thermal conductivity range between $K = 0.07 \text{ W m}^{-1}\text{K}^{-1}$ and $0.13 \text{ W m}^{-1}\text{K}^{-1}$, with the best-fit value $0.1 \text{ W m}^{-1}\text{K}^{-1}$. Equivalently, the value of thermal inertia is found to be between 310 and $420 \text{ J m}^{-2}\text{K}^{-1}\text{s}^{-1/2}$. This range of values is consistent with (or perhaps only slightly larger than) the thermal inertia values estimated in Delbò et al. (2007).

The confidence range of the c_{YORP} parameter is $0.4 - 1.1$, with the best-fit value of 0.72 . As discussed above such a value would be expected for a rough surface. It is also in a broad agreement with the results obtained for older asteroid families (e.g., Vokrouhlický et al. 2006a) and models of the pole and rotation rate distributions of small main-belt asteroids (e.g., Hanuš et al. 2011).

Figure 9 shows how the best-fit solution compares with the measured distribution of drift rates. The agreement is very good. A slight inconsistency arises in Fig. 9 because the measured profile shows more depletion in the central bins with $\Delta a \simeq 0 \text{ au}$. We suspect that this points to a slight inconsistency of the assumed dependency of the g function on ε for $\varepsilon \simeq 90^\circ$. Recall that Čapek & Vokrouhlický (2004) computed the g function for a specific collection of shapes. It is possible that the young, freshly re-accumulated asteroids in the Karin family have a different distribution of shapes. We leave this interesting problem for a future work.

Figure 10 shows the distribution of the initial and final values of the model rotation rates. We find that the small Karin members should still have roughly the same distribution of rotation rates as they had initially just after the family-formation event.

Above we adopted the bulk density $\rho_b = 2.5 \text{ g cm}^{-3}$. In the subsequent simulations we tested the dependence of the results on ρ_b and found that the best-fit solution scales as $K^* \propto 1/\rho_b^2$ and $c_{\text{YORP}}^* \propto \rho_b$ (the confidence regions recalibrate accordingly). The scaling of c_{YORP}^* arises from the YORP torque (inverse) dependence on body’s mass. The scaling of K^* is less transparent. It can be understood from the analysis of the Yarkovsky drift rate in semi-major axis given by Eq. (6). Note that in the relevant regime of large Θ values, $da/dt \propto 1/(\rho_b \Theta)$ and $\Theta \propto \sqrt{K}$. Therefore, to have the same value of drift rate da/dt , $\rho_b \sqrt{K}$ needs to be kept constant. This produces the aforementioned scaling of the results. The arrow in Fig. 8 indicates how the results would change if $\rho_b = 2 \text{ g cm}^{-3}$.

Finally, we verified that our best-fit solution obtained for the size interval I1 does not violate constraints from the interval I2. For that we used the best fit values of $(K, c_{\text{YORP}}, \delta_{\text{YORP}})$,

and re-run the simulations for $D = 3$ km, which is a characteristic size in I2. The modeled distribution of Δa_{model} was found to be consistent with the measured Δa values shown in Fig. 7 (bottom panel). We therefore confirm that the measured drift rates in I2 were not significantly affected by the YORP effect.

10. Numerical integration with the Yarkovsky effect and encounters with Ceres

The distribution of the semi-major axis drift rates were obtained in Sect. 3, where we used analytical arguments to improve the convergence of angles from a numerical simulation that ignored any drift. Here we include the semi-major axis drift directly in a numerical simulation to test how the convergence of angles is improved. In a separate simulation, we also include the gravitational effects of (1) Ceres to see how the convergence can be affected by close encounters of the Karin cluster members with Ceres.

We modified *SWIFT_RMVS3* (Levison & Duncan 1994) to include a semi-major axis drift (Nesvorný & Bottke 2004). For each of the confirmed Karin cluster members, we generated 13 clones with different drift rate values near the analytical estimate obtained in Sect. 3. The orbits of the clones were tracked backward in time for 10 My. We then checked which of the clones showed the best convergence of Ω and ϖ at $\tau = 5.746$ My. The drift rate assigned to the best clones is our best numerical estimate of the actual drift rate. On one hand, the numerical rate inferred here can be considered a better estimate of the true drift rates than the analytical method in Sect. 3. In practice, however, the resolution with a limited number of clones is not good enough to distinguish between differences in the drift rates that are of the order of 5%.

About 70% of the best clones converged to within $\pm 10^\circ$ in Ω and ϖ at $\tau = 5.746$ My. Their past orbital histories are shown in Fig. 11. The remaining 30% of the best clones converged as well, but not within $\pm 10^\circ$. This is contributed by the limited resolution of our numerical integration and/or, at least in some cases, by short-period oscillations of the osculating angles Ω and ϖ near the estimated family age. A more detailed study of this problem is left for future work.

Next we discuss the results obtained when (1) Ceres was included in the numerical integration. There are two ways that (1) Ceres can be influencing the results. First, a close encounter between a small asteroid and Ceres can lead to a change of the small body’s semi-major axis, which would then influence the measured drift rate. Second, the secular resonances with (1) Ceres (Novaković et al. 2015) can alter the precession rates of Ω and ϖ ,

and therefore influence the convergence of these angles as well. To determine which of these effects has a bigger weight, we monitored in the simulation all close encounters of all bodies with (1) Ceres.

Figure 12 compares the distribution of Ω values obtained for $\tau = 5.746$ My in our numerical simulations with and without Ceres (results for ϖ are similar). The distribution in the simulation with Ceres is clearly broader. We find that this is mainly a consequence of close encounters with Ceres. Of the 322 clones that converged within $\pm 10^\circ$ in a simulation without Ceres, roughly 80% converge within $\pm 10^\circ$ in a simulation with Ceres. The remaining 20% of the best clones do not converge so well. Of these, roughly 75% suffered close encounters to Ceres (within the Hill sphere or closer). A small fraction of clones suffered a very close Ceres encounter, and had $\Delta\Omega \simeq 30^\circ$ at $\tau = 5.746$ My. On average, Ceres encounters add $\simeq 4^\circ$ to the dispersion of angles at the time of convergence. This limits the precision to which the convergence of angles can be determined, and therefore the accuracy with which the Δa values over the estimated age of the family can be computed: a difference of 4° corresponds to a difference of 7.2×10^{-5} au in the Δa computed from the convergence of Ω and of 5.3×10^{-5} au for that from ϖ . Including other massive asteroids in the simulation would slightly increase this threshold.

11. Conclusions

The main results of this work can be summarized as follows:

- We revised the Karin family membership using the identification from Nesvorný et al. (2015) and initially including asteroids in the immediate neighborhood of the Karin cluster. The taxonomical and albedo interlopers were eliminated. We numerically integrated the orbits of all selected objects backward in time over 10 My. Using the convergence criteria described in the main text, we identified 576 asteroids that are very likely true members of the Karin cluster.
- Using the method of Nesvorný & Bottke (2004), we inferred the drift rates caused by the Yarkovsky effect. By minimizing the difference between two determinations of Δa from Ω and ϖ we found that the age of the Karin cluster is $\tau = 5.746 \pm 0.011$ My. This age determination is consistent with and improves on the previous estimate.
- Since the Yarkovsky drift rate depends on obliquity, we interpreted the observed distribution of the drift rates in terms of the obliquity distribution. For small, $D = 1\text{-}2$ km Karin cluster members, the distribution of obliquities is clearly bimodal. The best ex-

planation for such a distribution is that the YORP effect acted to alter the distribution that has been more uniform initially.

- We simulated the evolution of obliquities and spin rates with a simple Yarkovsky/YORP model. We found that the magnitude of the obliquity changes required to explain the bimodal distribution is consistent with the YORP effect and inferred age τ . The surface thermal conductivity is inferred to be $0.07 - 0.2 \text{ W m}^{-1} \text{ K}^{-1}$, corresponding to the thermal inertia of $\simeq 300 - 500 \text{ J m}^{-2} \text{ K}^{-1} \text{ s}^{-1/2}$). We find that the strength of the YORP effect is roughly $\simeq 0.7$ of the nominal strength obtained for a collection of random Gaussian spheroids. These results are consistent with a surface composed of rough, rocky regolith.
- We performed additional numerical simulations with the Yarkovsky drift and gravity of (1) Ceres. We found that the close encounters of Karin cluster members with Ceres act to increase the dispersion of angles and does not allow us, even in principle, to obtain a perfect convergence. On average, Ceres increases the dispersion of angles by $\sim 4^\circ$ at $\tau = 5.746 \text{ My}$.

Our work motivates new observational efforts. In particular, it would be interesting to verify the obliquity distribution inferred from our work. A decade ago such a goal would have been a remote possibility, but recent advancements in asteroid shape and rotation state studies can lead to interesting results soon. For example, the obliquities of individual bodies can be obtained from the sparse photometry data of ground-based survey programs (e.g., Āurech et al. 2016). Even more powerful results are expected from the space missions such as Gaia (e.g., Mignard et al. 2007).

Acknowledgments

We thank the reviewer of this paper, Dr. Bojan Novaković, for comments and suggestions that improved the quality of this work. This paper was written while the first author was a visiting scientist at the Southwest Research Institute (SwRI) in Boulder, CO, USA. We would like to thank the São Paulo State Science Foundation (FAPESP) that supported this work via the grant 14/24071-7. D.N.’s work on this project was supported by NASA’s Solar System Workings program, while D.V. was supported by the Czech Grant Agency (grant GA13-01308S). This publication makes use of data products from the Wide-field Infrared Survey Explorer (WISE) and from NEOWISE, which are a joint project of the University of California, Los Angeles, and the Jet Propulsion Laboratory/California Institute of Technology, funded by the National Aeronautics and Space Administration.

12. Appendix 1

In Table 1 we report the list of 480 identified Karin cluster members. The table lists their absolute magnitude, proper elements $(a_P, e_P, \sin i_P)$, frequencies g and s , Lyapunov exponents (Lyapunov exponents with values near $1.5 \times 10^{-6} yr^{-1}$ correspond to objects for which the integration time was not long enough to obtain a convergence), estimated mean obliquity ε , and estimated mean Yarkovsky drift speed. Note to observers: the obliquity values listed in Table 1 are historical mean obliquities and may not exactly coincide with the current values. Figure 13 shows the correspondence between the historical obliquity values given in Table 1 and our estimate of the present obliquities.

Table 1:: Karin cluster members: absolute magnitudes, proper elements and frequencies, Lyapunov exponents, and estimated mean obliquities and Yarkovsky drift speed.

Number	H	a_P [au]	e_P	$\sin i_P$	g_P " yr ⁻¹	s_P " yr ⁻¹	LCE 10 ⁻⁶ yr ⁻¹	ϵ [deg]	Drift speed [10 ⁻⁵ auMy ⁻¹]
832	11.18	2.86440	0.04390	0.03687	70.639	-65.235	1.49		
10783	13.41	2.86480	0.04411	0.03683	70.676	-65.270	1.49	113	-0.84
11728	13.48	2.86555	0.04443	0.03676	70.746	-65.334	1.56	180	-3.10
13765	14.41	2.86967	0.04585	0.03688	71.112	-65.667	1.15	180	-5.33
13807	13.68	2.86885	0.04527	0.03682	71.037	-65.590	1.92	162	-2.54
15649	14.70	2.86418	0.04393	0.03650	70.632	-65.226	1.47	180	-4.50
16706	14.43	2.86200	0.04330	0.03676	70.435	-65.051	1.49	180	-4.86
20089	14.76	2.86170	0.04312	0.03696	70.402	-65.022	1.46	139	-3.10
20095	14.44	2.86709	0.04478	0.03644	70.891	-65.457	1.49	137	-2.40
23054	14.78	2.86938	0.04553	0.03683	71.085	-65.636	1.49	56	2.00
23338	14.86	2.86781	0.04509	0.03734	70.930	-65.507	1.49	56	2.18
26970	14.93	2.86726	0.04473	0.03645	70.905	-65.466	1.49	54	2.35
28271	14.31	2.87018	0.04584	0.03683	71.159	-65.703	0.00	127	-1.86
33143	14.14	2.86831	0.04526	0.03751	70.969	-65.545	1.41	180	-6.31
34312	14.37	2.86857	0.04543	0.03679	71.015	-65.578	1.48	99	-0.60
35315	14.75	2.87056	0.04883	0.03651	71.230	-65.848	0.00	81	0.52
40782	14.55	2.86698	0.04477	0.03732	70.856	-65.439	1.49	98	-0.49
40789	14.74	2.86147	0.04305	0.03700	70.382	-65.004	1.50	180	-5.24
40921	14.37	2.86876	0.04526	0.03662	71.035	-65.586	1.48	77	0.79
41307	15.18	2.86604	0.04455	0.03651	70.797	-65.375	1.57	127	-2.80
43032	14.20	2.86616	0.04451	0.03687	70.796	-65.378	1.49	137	-2.07
45257	14.67	2.85934	0.04239	0.03601	70.228	-64.848	1.50	120	-1.84
47640	14.48	2.86498	0.04419	0.03687	70.691	-65.285	1.49	88	0.07
47866	15.24	2.86165	0.04301	0.03664	70.407	-65.019	1.49	60	2.31
48312	14.74	2.86111	0.04285	0.03661	70.361	-64.977	1.48	29	3.25
48369	14.62	2.86647	0.04446	0.03692	70.820	-65.396	1.49	0	4.74
50594	14.38	2.86494	0.04330	0.03657	70.688	-65.255	1.50	92	-0.14
50715	14.29	2.86592	0.04447	0.03667	70.780	-65.362	1.33	86	0.20
51068	14.62	2.86367	0.04375	0.03700	70.573	-65.179	1.49	145	-2.91
51089	14.77	2.87035	0.04593	0.03669	71.179	-65.720	1.31	79	0.68

Continued on next page

Table 1 – *Continued from previous page*

Number	H	a_P [au]	e_P	$\sin i_P$	g_P " yr ⁻¹	s_P " yr ⁻¹	LCE 10 ⁻⁶ yr ⁻¹	ϵ [deg]	Drift speed [10 ⁻⁵ auMy ⁻¹]
51923	15.09	2.86732	0.04501	0.03704	70.895	-65.473	1.49	180	-6.62
52009	15.15	2.86198	0.04338	0.03714	70.423	-65.048	1.50	180	-8.50
55124	14.97	2.86705	0.04492	0.03626	70.894	-65.461	1.49	97	-0.56
55852	15.49	2.86158	0.04307	0.03705	70.390	-65.012	1.48	79	0.98
56285	14.98	2.86542	0.04436	0.03650	70.742	-65.326	1.49	100	-0.67
57735	14.80	2.86625	0.04449	0.03689	70.802	-65.382	1.49	0	6.23
64165	15.14	2.86399	0.04391	0.03689	70.604	-65.208	1.49	180	-5.02
65383	15.69	2.86183	0.04298	0.03663	70.421	-65.030	1.48	41	4.35
65801	15.25	2.86306	0.04366	0.03634	70.540	-65.142	0.10	94	-0.40
69009	14.80	2.86516	0.04429	0.03668	70.714	-65.303	1.51	97	-0.47
69174	15.31	2.86237	0.04330	0.03643	70.475	-65.080	1.48	64	2.10
71003	14.89	2.86201	0.04327	0.03678	70.435	-65.050	1.49	62	1.63
71031	14.57	2.86532	0.04434	0.03735	70.708	-65.308	1.49	88	0.09
73950	15.23	2.86177	0.04315	0.03633	70.427	-65.035	1.49	95	-0.46
75176	15.72	2.86647	0.04457	0.03722	70.813	-65.397	1.49	74	1.59
75668	14.94	2.86453	0.04385	0.03688	70.650	-65.243	1.50	30	3.52
76686	14.77	2.86475	0.04407	0.03715	70.663	-65.262	1.48	97	-0.50
79035	14.54	2.86398	0.04391	0.03691	70.603	-65.207	1.49	159	-2.69
79213	14.70	2.86651	0.04455	0.03726	70.815	-65.398	1.47	76	0.84
82780	14.78	2.86786	0.04516	0.03697	70.945	-65.517	1.52	119	-1.85
84465	14.97	2.86546	0.04441	0.03739	70.719	-65.320	1.58	73	1.19
85350	15.17	2.86675	0.04469	0.03727	70.837	-65.420	1.49	62	2.12
87990	14.83	2.86415	0.04408	0.03649	70.631	-65.229	1.59	180	-6.53
88892	15.42	2.86090	0.04298	0.03647	70.348	-64.968	1.46	127	-3.13
89546	15.04	2.86677	0.04470	0.03705	70.845	-65.425	1.51	77	0.94
90640	15.22	2.86598	0.04472	0.03730	70.770	-65.368	1.49	180	-7.48
91694	15.09	2.86099	0.04293	0.03655	70.353	-64.972	1.55	149	-3.79
91706	14.89	2.86229	0.04346	0.03715	70.449	-65.072	1.50	154	-3.59
93632	15.14	2.86764	0.04485	0.03710	70.920	-65.489	1.49	16	4.30
93690	15.39	2.86802	0.04512	0.03727	70.950	-65.523	1.50	46	3.47
94089	14.46	2.86529	0.04435	0.03675	70.723	-65.313	1.49	81	0.48
95276	15.37	2.86326	0.04366	0.03613	70.563	-65.158	4.29	180	-7.66
97104	15.28	2.86612	0.04457	0.03631	70.810	-65.384	1.49	180	-5.29
97137	15.64	2.87071	0.04596	0.03647	71.218	-65.749	1.51	0	6.17

Continued on next page

Table 1 – *Continued from previous page*

Number	H	a_P [au]	e_P	$\sin i_P$	g_P " yr ⁻¹	s_P " yr ⁻¹	LCE 10 ⁻⁶ yr ⁻¹	ϵ [deg]	Drift speed [10 ⁻⁵ auMy ⁻¹]
100295	15.40	2.86781	0.04533	0.03680	70.947	-65.521	1.49	180	-5.92
103852	15.30	2.86799	0.04510	0.03664	70.966	-65.528	0.00	77	1.02
104409	15.16	2.86803	0.04526	0.03657	70.973	-65.537	1.43	125	-2.62
105265	15.16	2.86790	0.04511	0.03707	70.945	-65.516	1.49	109	-1.54
105324	15.12	2.86510	0.04423	0.03678	70.705	-65.296	1.48	29	3.47
105672	15.10	2.86807	0.04514	0.03676	70.970	-65.534	1.60	0	4.69
111335	15.55	2.86125	0.04319	0.03636	70.383	-65.001	1.62	165	-5.26
111436	15.02	2.86076	0.04297	0.03655	70.334	-64.958	0.90	135	-3.02
112776	16.03	2.86256	0.04341	0.03647	70.492	-65.097	1.50	55	3.85
112779	15.83	2.86182	0.04326	0.03652	70.427	-65.041	1.49	180	-9.30
114730	15.73	2.86471	0.04406	0.03724	70.657	-65.258	1.09	87	0.23
116288	15.23	2.86577	0.04429	0.03696	70.757	-65.341	0.77	0	7.37
116633	15.54	2.86642	0.04470	0.03727	70.808	-65.397	1.49	80	0.87
116653	15.57	2.86103	0.04305	0.03670	70.353	-64.977	1.99	180	-7.71
117482	15.55	2.86556	0.04443	0.03682	70.745	-65.334	1.31	126	-3.20
117761	15.44	2.86568	0.04435	0.03653	70.763	-65.343	6.69	87	0.19
118208	15.46	2.86730	0.04488	0.03667	70.904	-65.472	1.49	62	2.41
118841	15.46	2.86676	0.04448	0.03696	70.845	-65.417	1.59	0	5.59
119794	15.36	2.86573	0.04436	0.03684	70.758	-65.343	4.68	46	3.44
119818	15.46	2.86620	0.04458	0.03685	70.800	-65.383	1.49	154	-4.70
119861	15.57	2.86738	0.04493	0.03621	70.925	-65.485	1.49	88	0.16
120589	16.41	2.86819	0.04508	0.03719	70.967	-65.535	1.42	0	8.19
126465	15.40	2.86585	0.04440	0.03697	70.764	-65.350	0.20	47	3.45
126783	16.02	2.86607	0.04455	0.03614	70.810	-65.382	1.49	159	-6.30
126806	15.39	2.86375	0.04374	0.03714	70.575	-65.183	1.50	104	-1.25
126922	15.30	2.86753	0.04504	0.03670	70.924	-65.493	1.49	113	-1.92
126929	15.57	2.86615	0.04456	0.03630	70.812	-65.385	1.49	180	-5.95
128125	14.85	2.86702	0.04471	0.03654	70.881	-65.448	1.48	23	3.61
128214	15.32	2.86147	0.04303	0.03638	70.400	-65.010	1.48	112	-1.84
128297	15.57	2.86720	0.04472	0.03668	70.893	-65.460	1.51	70	1.81
128333	15.36	2.86221	0.04334	0.03663	70.457	-65.069	1.49	121	-2.61
128932	16.25	2.87184	0.04743	0.03633	71.335	-65.885	1.49	180	-7.93
128944	15.41	2.86283	0.04362	0.03714	70.496	-65.115	1.49	159	-4.77
129268	15.91	2.86255	0.04330	0.03644	70.490	-65.092	1.51	0	6.46

Continued on next page

Table 1 – *Continued from previous page*

Number	H	a_P [au]	e_P	$\sin i_P$	g_P " yr ⁻¹	s_P " yr ⁻¹	LCE 10 ⁻⁶ yr ⁻¹	ϵ [deg]	Drift speed [10 ⁻⁵ auMy ⁻¹]
129691	16.02	2.86965	0.04562	0.03666	71.115	-65.660	1.72	56	3.74
130232	16.04	2.85937	0.04265	0.03668	70.213	-64.851	1.49	180	-10.18
131987	15.09	2.86071	0.04269	0.03661	70.326	-64.944	1.39	114	-1.81
133275	15.98	2.86195	0.04319	0.03631	70.443	-65.049	1.49	90	-0.11
133478	16.10	2.86637	0.04464	0.03734	70.801	-65.391	1.48	99	-1.17
134155	16.05	2.86268	0.04380	0.03630	70.510	-65.121	1.49	180	-8.75
134183	15.63	2.86642	0.04446	0.03666	70.824	-65.396	1.49	57	2.99
139578	15.35	2.86159	0.04314	0.03701	70.392	-65.015	1.48	180	-7.05
139639	15.36	2.86684	0.04476	0.03635	70.872	-65.440	1.50	141	-3.90
139916	14.98	2.86363	0.04381	0.03686	70.574	-65.180	1.50	118	-1.97
140153	16.11	2.86191	0.04331	0.03697	70.422	-65.043	1.48	130	-4.57
140155	15.34	2.86639	0.04454	0.03717	70.807	-65.391	1.49	45	3.45
140157	15.44	2.86798	0.04510	0.03701	70.954	-65.522	1.49	73	1.43
140337	16.39	2.86730	0.04466	0.03664	70.902	-65.464	1.49	18	7.56
140602	16.25	2.86493	0.04432	0.03601	70.714	-65.296	1.50	130	-4.83
140778	16.36	2.86736	0.04489	0.03649	70.914	-65.479	1.49	45	5.57
140863	15.95	2.86066	0.04293	0.03670	70.322	-64.948	1.27	180	-6.72
142988	15.68	2.86178	0.04328	0.03586	70.442	-65.046	1.50	141	-4.52
143155	16.05	2.86744	0.04488	0.03639	70.924	-65.485	1.49	70	2.27
143711	15.71	2.86381	0.04370	0.03681	70.590	-65.189	1.49	66	2.34
144484	15.69	2.86471	0.04407	0.03681	70.669	-65.263	1.48	93	-0.31
145516	15.39	2.86705	0.04465	0.03679	70.876	-65.445	1.49	75	1.24
146704	15.57	2.86701	0.04464	0.03680	70.872	-65.442	1.45	64	2.33
146783	15.58	2.86594	0.04450	0.03710	70.770	-65.359	1.48	59	2.82
149908	16.30	2.86771	0.04501	0.03663	70.941	-65.505	1.49	63	3.39
149942	16.06	2.86442	0.04410	0.03732	70.629	-65.238	1.46	160	-6.47
151300	15.34	2.86300	0.04354	0.03698	70.514	-65.126	1.39	180	-7.52
152430	16.61	2.86831	0.04516	0.03709	70.981	-65.547	1.40	47	5.93
152487	16.05	2.86050	0.04300	0.03665	70.311	-64.940	1.62	180	-10.64
154046	15.03	2.86555	0.04452	0.03686	70.743	-65.335	1.58	126	-2.55
154097	16.45	2.86156	0.04298	0.03619	70.412	-65.017	1.48	52	4.99
154104	16.15	2.86796	0.04502	0.03635	70.971	-65.526	1.72	37	5.67
154114	15.58	2.86471	0.04417	0.03681	70.670	-65.266	1.49	135	-3.95
155170	16.17	2.86427	0.04379	0.03696	70.625	-65.222	1.51	74	1.87

Continued on next page

Table 1 – *Continued from previous page*

Number	H	a_P [au]	e_P	$\sin i_P$	g_P " yr ⁻¹	s_P " yr ⁻¹	LCE 10 ⁻⁶ yr ⁻¹	ϵ [deg]	Drift speed [10 ⁻⁵ auMy ⁻¹]
186242	15.79	2.86569	0.04432	0.03662	70.761	-65.341	4.46	45	4.22
187169	16.81	2.85886	0.04201	0.03603	70.186	-64.803	1.49	57	5.20
187223	16.77	2.87108	0.04615	0.03681	71.242	-65.777	1.49	0	10.12
187593	16.49	2.86201	0.04336	0.03665	70.440	-65.055	1.49	145	-6.85
188913	16.96	2.86872	0.04532	0.03665	71.031	-65.586	1.52	80	1.75
189477	16.55	2.86510	0.04418	0.03596	70.728	-65.303	1.49	46	5.88
191769	16.32	2.86131	0.04300	0.03641	70.385	-64.997	1.50	136	-5.65
192554	16.10	2.86953	0.04533	0.03651	71.106	-65.643	1.48	0	7.41
192702	16.01	2.86457	0.04419	0.03651	70.667	-65.261	1.49	159	-6.30
192868	16.50	2.86179	0.04323	0.03692	70.412	-65.033	1.49	83	0.93
192993	16.41	2.86175	0.04334	0.03708	70.405	-65.032	1.48	180	-9.99
196023	15.78	2.86582	0.04432	0.03656	70.773	-65.350	1.32	0	6.45
196739	15.19	2.86357	0.04368	0.03705	70.562	-65.169	1.58	50	2.95
196886	15.85	2.86595	0.04454	0.03739	70.762	-65.357	1.48	109	-2.04
198656	15.82	2.86001	0.04270	0.03680	70.263	-64.895	1.49	114	-2.54
199314	16.68	2.86785	0.04502	0.03660	70.955	-65.516	1.52	29	7.95
199416	15.99	2.86836	0.04516	0.03737	70.977	-65.547	1.07	53	3.91
199465	15.73	2.87275	0.04807	0.03596	71.433	-65.977	1.85	80	0.99
199496	15.78	2.87053	0.04604	0.03682	71.191	-65.735	1.61	57	3.23
199617	16.03	2.86539	0.04425	0.03651	70.738	-65.319	1.49	54	3.94
200297	15.66	2.86555	0.04452	0.03650	70.754	-65.340	1.98	135	-4.08
200306	16.13	2.86826	0.04521	0.03724	70.972	-65.543	1.66	69	2.47
201209	16.41	2.86015	0.04284	0.03687	70.274	-64.908	1.49	180	-10.09
201647	16.77	2.86169	0.04313	0.03710	70.397	-65.020	1.54	121	-4.92
201659	16.49	2.86111	0.04305	0.03726	70.344	-64.976	1.50	180	-10.53
201717	15.71	2.86932	0.04548	0.03673	71.083	-65.631	1.34	129	-3.67
202595	16.24	2.86620	0.04450	0.03666	70.805	-65.383	1.49	123	-4.10
203797	16.10	2.86393	0.04385	0.03700	70.595	-65.200	1.49	131	-4.61
204075	15.76	2.85991	0.04265	0.03619	70.272	-64.894	1.42	98	-0.86
204090	16.16	2.86751	0.04477	0.03783	70.886	-65.469	1.49	146	-6.01
204602	16.31	2.86734	0.04501	0.03638	70.917	-65.483	1.49	131	-5.11
204735	16.27	2.87001	0.04550	0.03756	71.119	-65.670	1.55	65	3.13
204846	16.30	2.86785	0.04501	0.03655	70.956	-65.516	1.50	65	3.22
204866	16.04	2.86702	0.04479	0.03655	70.882	-65.451	1.50	122	-3.64

Continued on next page

Table 1 – *Continued from previous page*

Number	H	a_P [au]	e_P	$\sin i_P$	g_P " yr ⁻¹	s_P " yr ⁻¹	LCE 10 ⁻⁶ yr ⁻¹	ϵ [deg]	Drift speed [10 ⁻⁵ auMy ⁻¹]
204897	16.45	2.86449	0.04400	0.03625	70.666	-65.252	1.49	104	-2.05
204944	16.32	2.86438	0.04405	0.03589	70.668	-65.250	1.49	130	-5.03
205016	16.32	2.86765	0.04486	0.03637	70.942	-65.498	1.49	35	6.32
206023	16.15	2.86700	0.04461	0.03727	70.857	-65.434	1.49	0	12.19
206172	16.14	2.86120	0.04313	0.03670	70.369	-64.991	1.50	180	-9.04
206759	15.96	2.85950	0.04267	0.03586	70.248	-64.869	1.49	165	-6.33
207613	15.94	2.86371	0.04387	0.03701	70.577	-65.186	1.49	180	-6.68
207690	16.46	2.86157	0.04317	0.03627	70.412	-65.023	1.49	167	-8.04
207758	16.00	2.86813	0.04507	0.03720	70.961	-65.529	0.05	39	5.16
209894	16.05	2.86733	0.04498	0.03597	70.927	-65.485	1.49	118	-3.22
209990	16.42	2.86680	0.04459	0.03657	70.861	-65.428	1.49	48	5.32
211843	16.37	2.86693	0.04472	0.03611	70.886	-65.447	1.58	97	-1.00
212304	16.24	2.86557	0.04460	0.03737	70.730	-65.334	0.83	116	-3.37
212562	16.47	2.86602	0.04442	0.03658	70.791	-65.368	1.51	64	3.63
212896	16.06	2.86015	0.04273	0.03709	70.266	-64.902	1.50	150	-5.99
213350	16.15	2.86908	0.04523	0.03655	71.065	-65.608	1.49	15	6.90
214835	16.30	2.86971	0.04564	0.03765	71.090	-65.653	1.49	0	10.69
218061	15.66	2.86500	0.04416	0.03667	70.699	-65.288	1.49	50	3.64
218459	16.51	2.86834	0.04518	0.03726	70.979	-65.547	1.49	45	5.90
219904	15.65	2.86212	0.04331	0.03676	70.445	-65.059	1.49	122	-3.07
220792	16.08	2.86803	0.04502	0.03699	70.958	-65.523	1.61	26	6.20
221213	16.48	2.86688	0.04482	0.03696	70.858	-65.438	1.49	125	-4.80
221487	15.57	2.86168	0.04324	0.03629	70.422	-65.033	1.49	137	-4.04
221754	15.95	2.86808	0.04512	0.03740	70.952	-65.526	0.97	83	0.78
221781	15.85	2.86672	0.04459	0.03677	70.848	-65.420	1.50	96	-0.73
223767	16.55	2.86420	0.04373	0.03602	70.646	-65.226	1.57	52	5.19
223792	16.50	2.86645	0.04448	0.03716	70.811	-65.392	1.49	46	5.82
223813	16.24	2.86667	0.04446	0.03608	70.862	-65.420	1.49	67	2.84
223920	16.36	2.86311	0.04383	0.03692	70.528	-65.144	0.09	180	-8.50
224603	16.48	2.86213	0.04348	0.03679	70.446	-65.066	1.50	180	-8.76
224605	16.83	2.86197	0.04323	0.03661	70.436	-65.048	1.49	94	-0.71
224611	16.75	2.86654	0.04469	0.03612	70.852	-65.419	1.54	130	-6.17
224946	15.85	2.86507	0.04423	0.03649	70.710	-65.296	1.49	64	2.68
225387	15.82	2.86314	0.04367	0.03706	70.525	-65.139	1.19	96	-0.65

Continued on next page

Table 1 – *Continued from previous page*

Number	H	a_P [au]	e_P	$\sin i_P$	g_P " yr ⁻¹	s_P " yr ⁻¹	LCE 10 ⁻⁶ yr ⁻¹	ϵ [deg]	Drift speed [10 ⁻⁵ auMy ⁻¹]
225392	16.69	2.86761	0.04478	0.03641	70.937	-65.493	1.49	52	5.64
226814	15.86	2.86387	0.04393	0.03719	70.585	-65.197	1.49	142	-4.98
226877	16.18	2.86468	0.04398	0.03686	70.664	-65.258	1.49	51	4.51
226916	16.12	2.86925	0.04528	0.03654	71.080	-65.622	1.49	0	12.66
227520	17.15	2.85874	0.04231	0.03642	70.167	-64.800	1.49	180	-11.82
227655	16.49	2.86612	0.04433	0.03661	70.798	-65.371	1.50	50	5.33
227658	16.30	2.86439	0.04398	0.03685	70.640	-65.238	1.49	114	-3.12
227708	15.40	2.86530	0.04434	0.03691	70.719	-65.311	1.49	79	0.92
229612	16.26	2.87001	0.04560	0.03668	71.146	-65.684	1.92	25	6.78
229621	15.95	2.86764	0.04499	0.03710	70.921	-65.494	1.49	99	-1.10
229702	15.95	2.85975	0.04264	0.03663	70.246	-64.877	1.51	123	-3.59
231307	16.83	2.86717	0.04475	0.03708	70.879	-65.453	1.48	69	3.40
231541	16.71	2.86742	0.04509	0.03735	70.895	-65.479	1.49	139	-7.03
231585	16.52	2.86885	0.04499	0.03758	71.012	-65.572	0.99	59	4.26
231788	16.47	2.86831	0.04506	0.03731	70.973	-65.540	1.51	29	7.18
233412	16.22	2.86649	0.04407	0.03756	70.799	-65.376	1.49	109	-2.47
233465	16.40	2.86003	0.04275	0.03658	70.271	-64.900	1.41	114	-3.31
233686	16.50	2.86057	0.04301	0.03719	70.301	-64.939	1.55	180	-11.48
233753	16.82	2.86096	0.04305	0.03721	70.332	-64.966	1.42	122	-5.29
235403	16.04	2.86597	0.04450	0.03714	70.771	-65.360	1.47	105	-1.85
236596	16.71	2.86109	0.04306	0.03714	70.345	-64.976	1.59	140	-7.13
236805	16.20	2.86454	0.04394	0.03730	70.639	-65.242	1.49	80	1.23
236834	16.57	2.86113	0.04298	0.03668	70.361	-64.982	1.49	121	-4.54
238014	16.50	2.86740	0.04470	0.03669	70.910	-65.472	1.51	45	5.91
238721	16.45	2.86063	0.04301	0.03682	70.316	-64.947	1.27	115	-3.52
239201	16.37	2.86057	0.04291	0.03682	70.310	-64.939	1.48	180	-9.51
239454	16.48	2.86093	0.04304	0.03714	70.332	-64.965	1.36	180	-9.46
240475	16.45	2.86342	0.04344	0.03715	70.542	-65.149	1.13	46	5.68
240687	16.95	2.87008	0.04555	0.03648	71.157	-65.689	0.68	21	9.62
241502	16.29	2.86834	0.04527	0.03694	70.989	-65.554	1.49	55	4.31
243171	16.38	2.85980	0.04279	0.03647	70.256	-64.887	1.47	180	-8.80
246677	16.57	2.86178	0.04333	0.03670	70.419	-65.038	1.49	146	-7.27
250705	16.57	2.86153	0.04312	0.03643	70.404	-65.017	1.46	180	-8.97
250735	15.58	2.86962	0.04829	0.03629	71.148	-65.765	1.46	57	2.93

Continued on next page

Table 1 – *Continued from previous page*

Number	H	a_P [au]	e_P	$\sin i_P$	g_P " yr ⁻¹	s_P " yr ⁻¹	LCE 10 ⁻⁶ yr ⁻¹	ϵ [deg]	Drift speed [10 ⁻⁵ auMy ⁻¹]
251300	16.21	2.86676	0.04469	0.03633	70.865	-65.432	1.50	180	-8.08
251526	15.93	2.86830	0.04508	0.03739	70.970	-65.539	1.54	35	5.25
254809	16.54	2.86495	0.04406	0.03707	70.681	-65.276	1.49	37	6.80
255109	16.34	2.86164	0.04327	0.03660	70.410	-65.028	1.49	157	-7.23
255336	16.33	2.86553	0.04456	0.03653	70.752	-65.339	0.00	180	-8.38
256438	16.87	2.86511	0.04404	0.03586	70.730	-65.300	1.50	29	8.66
256912	16.52	2.86619	0.04452	0.03738	70.782	-65.373	1.50	83	1.01
257004	16.80	2.86705	0.04456	0.03709	70.866	-65.438	1.49	48	6.38
257049	16.70	2.86686	0.04487	0.03652	70.869	-65.443	1.47	148	-7.85
257111	16.97	2.86378	0.04379	0.03608	70.609	-65.199	1.49	115	-4.48
257241	16.60	2.86744	0.04469	0.03682	70.909	-65.472	1.49	14	8.51
257509	16.83	2.86784	0.04493	0.03638	70.959	-65.514	1.50	42	7.17
258560	15.78	2.86845	0.04510	0.03702	70.994	-65.554	1.50	44	4.30
258677	16.00	2.86612	0.04453	0.03671	70.797	-65.377	1.49	55	3.74
260850	16.58	2.86699	0.04460	0.03687	70.868	-65.438	1.49	82	1.11
260875	16.65	2.86229	0.04325	0.03720	70.446	-65.064	1.49	74	2.35
261173	16.98	2.86327	0.04381	0.03610	70.566	-65.164	7.72	180	-13.31
261620	16.89	2.86439	0.04372	0.03626	70.655	-65.236	1.49	0	10.77
261625	16.38	2.86954	0.04529	0.03599	71.122	-65.649	1.48	0	9.98
262067	16.72	2.87021	0.04630	0.03701	71.160	-65.721	0.12	180	-11.67
262517	16.95	2.86630	0.04440	0.03639	70.821	-65.388	1.49	53	6.20
262608	16.48	2.86502	0.04410	0.03700	70.690	-65.283	1.47	51	5.14
262989	16.34	2.86501	0.04452	0.03624	70.715	-65.306	1.49	180	-9.91
263000	16.34	2.86248	0.04351	0.03671	70.478	-65.092	1.50	135	-5.54
264038	16.61	2.86673	0.04488	0.03641	70.861	-65.436	1.50	180	-10.42
265401	16.75	2.86797	0.04490	0.03638	70.970	-65.522	1.50	0	12.28
265412	16.48	2.86381	0.04389	0.03653	70.599	-65.199	1.49	180	-8.66
265862	16.69	2.85889	0.04239	0.03653	70.177	-64.811	1.49	180	-9.42
265919	16.52	2.86997	0.04547	0.03648	71.147	-65.679	1.29	0	10.43
266430	16.57	2.86499	0.04489	0.03760	70.676	-65.301	1.50	22	8.03
266842	16.38	2.86745	0.04485	0.03616	70.931	-65.487	1.49	53	4.75
268562	16.19	2.86708	0.04469	0.03729	70.864	-65.443	1.49	39	5.63
268583	16.15	2.86889	0.04467	0.03751	71.014	-65.564	1.49	134	-4.98
268631	16.98	2.85903	0.04243	0.03628	70.196	-64.825	1.49	146	-8.74

Continued on next page

Table 1 – *Continued from previous page*

Number	H	a_P [au]	e_P	$\sin i_P$	g_P " yr ⁻¹	s_P " yr ⁻¹	LCE 10 ⁻⁶ yr ⁻¹	ϵ [deg]	Drift speed [10 ⁻⁵ auMy ⁻¹]
269223	15.89	2.86816	0.04523	0.03693	70.973	-65.540	1.33	65	2.68
272451	16.04	2.86634	0.04459	0.03652	70.822	-65.397	1.49	110	-2.40
272971	16.79	2.86732	0.04462	0.03650	70.907	-65.466	1.50	0	9.75
272994	16.38	2.86040	0.04307	0.03714	70.288	-64.930	1.49	180	-9.56
273014	16.12	2.86363	0.04382	0.03734	70.560	-65.175	1.49	91	-0.20
273049	16.49	2.86735	0.04565	0.03779	70.880	-65.490	1.49	8	8.27
273052	16.83	2.86419	0.04424	0.03632	70.641	-65.239	1.49	180	-13.28
273138	16.72	2.86548	0.04436	0.03650	70.746	-65.329	1.48	78	1.81
274350	16.78	2.86430	0.04368	0.03680	70.631	-65.222	1.49	56	5.30
275058	16.79	2.86410	0.04404	0.03616	70.636	-65.228	1.49	113	-3.78
278304	16.89	2.86330	0.04374	0.03608	70.566	-65.164	0.67	119	-4.98
278760	16.56	2.86118	0.04295	0.03641	70.374	-64.987	1.46	127	-5.27
278810	16.95	2.86246	0.04308	0.03737	70.453	-65.067	1.49	38	8.11
278856	16.50	2.86760	0.04527	0.03676	70.930	-65.505	1.49	151	-7.40
279509	16.91	2.85986	0.04296	0.03657	70.260	-64.896	1.49	180	-11.82
280158	16.78	2.86809	0.04558	0.03767	70.949	-65.540	2.45	68	3.46
281843	16.58	2.86460	0.04445	0.03594	70.688	-65.278	1.66	180	-10.04
283094	16.79	2.86850	0.04519	0.03674	71.008	-65.564	1.53	45	6.75
283120	15.63	2.86560	0.04438	0.03656	70.755	-65.338	1.77	52	3.44
283891	17.01	2.87060	0.04585	0.03671	71.199	-65.733	0.64	0	11.89
284236	16.43	2.86685	0.04461	0.03730	70.843	-65.423	1.48	45	5.68
286577	16.44	2.85963	0.04266	0.03650	70.240	-64.871	1.48	159	-7.68
287022	17.09	2.86133	0.04330	0.03665	70.382	-65.007	1.49	180	-13.26
289418	16.95	2.86447	0.04418	0.03629	70.665	-65.256	1.50	146	-8.63
289659	16.43	2.86779	0.04495	0.03648	70.952	-65.510	1.49	0	8.80
290117	15.97	2.85962	0.04256	0.03617	70.248	-64.871	1.49	132	-4.48
290317	16.90	2.86407	0.04410	0.03612	70.635	-65.228	1.53	147	-8.56
290570	16.88	2.86106	0.04308	0.03695	70.349	-64.977	2.90	145	-8.24
290641	16.67	2.86239	0.04320	0.03633	70.479	-65.079	1.49	34	7.45
290705	17.08	2.86826	0.04599	0.03552	71.030	-65.592	1.37	75	2.82
291169	16.50	2.86605	0.04439	0.03631	70.801	-65.372	1.49	42	6.17
292634	17.15	2.86371	0.04389	0.03719	70.571	-65.184	1.49	145	-9.37
292678	16.94	2.85844	0.04224	0.03652	70.139	-64.776	1.48	126	-6.11
293364	16.75	2.87020	0.04560	0.03645	71.169	-65.700	0.12	11	9.22

Continued on next page

Table 1 – *Continued from previous page*

Number	H	a_P [au]	e_P	$\sin i_P$	g_P " yr ⁻¹	s_P " yr ⁻¹	LCE 10 ⁻⁶ yr ⁻¹	ϵ [deg]	Drift speed [10 ⁻⁵ auMy ⁻¹]
293432	16.77	2.86792	0.04486	0.03761	70.928	-65.502	1.56	0	9.67
294039	16.76	2.86882	0.04463	0.03759	71.005	-65.556	1.48	90	-0.09
294173	16.72	2.86133	0.04304	0.03631	70.390	-65.002	1.49	143	-7.46
294380	16.94	2.86553	0.04413	0.03641	70.751	-65.326	2.70	0	11.59
294924	16.57	2.86817	0.04500	0.03715	70.966	-65.530	4.84	0	9.03
295026	16.07	2.86882	0.04534	0.03695	71.031	-65.590	1.37	0	8.91
296025	16.59	2.87088	0.04597	0.03648	71.232	-65.760	1.48	0	9.94
296279	16.27	2.86585	0.04457	0.03642	70.782	-65.364	0.07	163	-7.24
296335	16.34	2.85857	0.04231	0.03653	70.150	-64.787	1.49	149	-6.73
296363	16.09	2.86254	0.04346	0.03716	70.469	-65.089	1.49	118	-3.37
296703	16.98	2.86979	0.04563	0.03682	71.123	-65.668	1.40	74	2.72
297115	17.03	2.86701	0.04456	0.03664	70.876	-65.441	1.46	67	4.11
297130	16.40	2.86126	0.04298	0.03637	70.381	-64.994	0.98	98	-1.23
297572	15.83	2.86412	0.04384	0.03668	70.620	-65.216	1.49	64	2.65
298678	16.45	2.86421	0.04393	0.03704	70.618	-65.222	1.49	125	-4.72
299751	16.75	2.86685	0.04461	0.03621	70.876	-65.437	1.51	75	2.37
299855	16.72	2.86084	0.04299	0.03711	70.325	-64.957	1.31	135	-6.63
300861	16.39	2.86531	0.04439	0.03677	70.724	-65.315	1.59	145	-6.61
300942	16.48	2.86960	0.04564	0.03644	71.117	-65.660	1.49	112	-3.17
301242	16.73	2.86812	0.04500	0.03654	70.979	-65.534	2.05	16	8.95
301400	16.55	2.86298	0.04361	0.03616	70.537	-65.137	1.73	163	-8.23
301440	16.16	2.86563	0.04422	0.03692	70.746	-65.330	3.14	35	5.83
301545	16.12	2.86191	0.04341	0.03683	70.426	-65.048	1.49	180	-9.90
302127	16.35	2.86338	0.04375	0.03645	70.564	-65.165	5.54	129	-4.96
302779	16.76	2.86243	0.04346	0.03620	70.489	-65.093	1.49	124	-5.34
304269	16.67	2.86126	0.04306	0.03656	70.376	-64.994	0.68	137	-6.70
304338	17.03	2.86510	0.04409	0.03626	70.718	-65.297	1.50	0	11.11
304385	16.81	2.86676	0.04463	0.03629	70.866	-65.430	1.43	86	0.57
304398	17.11	2.86701	0.04506	0.03669	70.879	-65.458	1.49	180	-11.37
308985	16.36	2.85960	0.04257	0.03718	70.217	-64.858	1.49	95	-0.73
308995	17.07	2.86731	0.04460	0.03680	70.898	-65.461	1.49	75	2.72
309049	17.31	2.86509	0.04418	0.03723	70.690	-65.288	1.49	74	3.20
309059	16.44	2.86095	0.04296	0.03642	70.354	-64.971	1.05	90	-0.06
309104	16.74	2.86700	0.04450	0.03626	70.886	-65.443	1.49	63	4.12

Continued on next page

Table 1 – *Continued from previous page*

Number	H	a_P [au]	e_P	$\sin i_P$	g_P " yr ⁻¹	s_P " yr ⁻¹	LCE 10 ⁻⁶ yr ⁻¹	ϵ [deg]	Drift speed [10 ⁻⁵ auMy ⁻¹]
309627	16.67	2.85940	0.04256	0.03719	70.200	-64.844	1.49	180	-10.61
310199	16.77	2.85865	0.04224	0.03670	70.151	-64.788	1.49	118	-4.48
312724	16.99	2.86317	0.04378	0.03720	70.524	-65.143	3.15	180	-14.02
314291	16.89	2.86699	0.04463	0.03709	70.862	-65.436	1.51	35	8.23
314389	16.78	2.87087	0.04617	0.03670	71.226	-65.765	1.49	180	-11.16
314428	16.84	2.86588	0.04462	0.03652	70.783	-65.367	0.34	180	-11.37
315038	17.09	2.85925	0.04252	0.03677	70.200	-64.838	1.50	135	-7.87
315783	16.75	2.86604	0.04432	0.03657	70.792	-65.366	1.50	0	12.56
315784	17.00	2.86326	0.04367	0.03687	70.541	-65.149	4.57	64	4.54
316354	16.79	2.86685	0.04490	0.03720	70.849	-65.436	1.50	138	-7.18
316368	17.03	2.86702	0.04449	0.03643	70.882	-65.441	1.51	37	8.48
316407	17.08	2.86254	0.04314	0.03700	70.471	-65.080	1.49	44	7.82
317243	17.25	2.86517	0.04434	0.03683	70.710	-65.303	1.50	108	-3.69
317372	16.77	2.86339	0.04379	0.03614	70.575	-65.171	5.99	116	-4.21
317556	16.70	2.86702	0.04487	0.03656	70.882	-65.454	1.50	142	-7.28
318989	17.02	2.86803	0.04500	0.03631	70.978	-65.530	1.48	45	7.42
319043	16.92	2.86511	0.04415	0.03676	70.705	-65.294	1.50	68	3.71
319079	16.55	2.86465	0.04404	0.03706	70.656	-65.255	1.49	67	3.23
319246	16.83	2.86189	0.04307	0.03642	70.433	-65.040	1.49	30	8.42
319424	16.74	2.86627	0.04470	0.03666	70.814	-65.395	1.49	128	-5.88
319975	16.63	2.86255	0.04365	0.03708	70.475	-65.098	1.49	143	-7.14
321522	16.73	2.86711	0.04458	0.03646	70.891	-65.451	1.48	36	7.55
322065	16.21	2.86411	0.04377	0.03703	70.609	-65.209	1.49	70	2.50
322142	17.32	2.86173	0.04303	0.03665	70.413	-65.025	1.49	82	1.69
322394	16.57	2.86903	0.04559	0.03646	71.066	-65.619	1.51	180	-9.60
324019	16.77	2.86223	0.04344	0.03674	70.456	-65.072	1.49	180	-9.79
324682	16.57	2.86514	0.04401	0.03700	70.700	-65.289	1.49	0	10.44
324716	17.06	2.86120	0.04320	0.03621	70.384	-65.000	1.68	180	-11.76
325474	17.03	2.86740	0.04477	0.03624	70.923	-65.479	1.49	51	6.63
326187	17.22	2.86200	0.04339	0.03714	70.425	-65.050	1.49	119	-5.81
326260	16.51	2.87088	0.04608	0.03669	71.227	-65.762	1.49	65	3.47
327003	16.77	2.86077	0.04299	0.03640	70.340	-64.961	1.48	180	-11.22
327486	17.08	2.86721	0.04450	0.03675	70.889	-65.450	1.48	0	12.55
330080	17.08	2.86121	0.04316	0.03655	70.374	-64.995	1.51	130	-7.06

Continued on next page

Table 1 – *Continued from previous page*

Number	H	a_P [au]	e_P	$\sin i_P$	g_P " yr ⁻¹	s_P " yr ⁻¹	LCE 10 ⁻⁶ yr ⁻¹	ϵ [deg]	Drift speed [10 ⁻⁵ auMy ⁻¹]
331824	16.94	2.86723	0.04502	0.03657	70.901	-65.473	1.49	137	-7.62
332163	16.61	2.86263	0.04336	0.03652	70.496	-65.099	1.50	60	4.35
332550	16.49	2.86743	0.04492	0.03700	70.906	-65.479	1.48	101	-1.61
332761	16.83	2.86533	0.04409	0.03565	70.755	-65.319	1.43	0	11.38
333383	16.68	2.86124	0.04319	0.03738	70.352	-64.988	1.52	180	-9.43
335618	16.90	2.86541	0.04437	0.03583	70.760	-65.333	1.49	83	1.06
336438	17.03	2.86146	0.04289	0.03640	70.397	-65.005	1.50	82	1.32
336910	16.38	2.86827	0.04515	0.03695	70.981	-65.544	1.50	98	-1.20
339406	16.79	2.86608	0.04445	0.03726	70.776	-65.365	1.15	52	5.80
339447	16.57	2.86757	0.04480	0.03654	70.930	-65.489	1.49	39	6.68
339474	16.08	2.86247	0.04358	0.03712	70.466	-65.089	1.49	180	-8.82
339476	15.69	2.86269	0.04355	0.03681	70.494	-65.107	1.49	137	-4.23
341166	16.73	2.86104	0.04315	0.03647	70.362	-64.983	1.49	180	-14.28
341250	16.62	2.86647	0.04443	0.03711	70.814	-65.393	1.49	15	8.56
341298	16.71	2.86772	0.04501	0.03602	70.960	-65.513	1.49	81	1.33
341350	16.93	2.85929	0.04222	0.03648	70.210	-64.834	1.49	47	6.89
341565	16.87	2.86556	0.04432	0.03678	70.745	-65.330	1.82	48	6.54
343584	16.61	2.85942	0.04255	0.03631	70.227	-64.855	1.49	146	-7.33
344811	17.12	2.85944	0.04267	0.03595	70.241	-64.865	1.48	164	-10.78
346024	16.70	2.86708	0.04468	0.03683	70.878	-65.447	1.49	53	5.51
346031	16.76	2.86767	0.04489	0.03643	70.943	-65.501	1.53	19	8.95
346559	16.26	2.85952	0.04262	0.03679	70.223	-64.859	1.48	180	-8.71
346731	16.89	2.86518	0.04445	0.03628	70.728	-65.314	1.50	107	-3.00
348534	17.08	2.86370	0.04363	0.03646	70.590	-65.183	1.49	71	3.48
348611	16.75	2.85963	0.04283	0.03708	70.225	-64.870	1.49	180	-14.66
348963	16.75	2.86888	0.04534	0.03665	71.046	-65.598	1.50	49	6.12
349261	17.05	2.86692	0.04482	0.03605	70.888	-65.450	1.51	127	-6.58
349332	17.14	2.85968	0.04230	0.03608	70.253	-64.867	1.50	58	5.87
349348	16.95	2.86740	0.04468	0.03733	70.891	-65.464	1.50	0	13.11
349384	17.04	2.86800	0.04517	0.03720	70.951	-65.524	1.60	61	5.15
350308	16.63	2.85893	0.04238	0.03596	70.197	-64.821	1.49	168	-8.75
351888	16.73	2.86781	0.04483	0.03633	70.957	-65.509	1.49	0	10.54
352470	16.61	2.86303	0.04352	0.03730	70.507	-65.123	0.91	52	5.36
353480	16.55	2.86537	0.04407	0.03677	70.726	-65.309	1.51	0	9.94

Continued on next page

Table 1 – *Continued from previous page*

Number	H	a_P [au]	e_P	$\sin i_P$	g_P " yr ⁻¹	s_P " yr ⁻¹	LCE 10 ⁻⁶ yr ⁻¹	ϵ [deg]	Drift speed [10 ⁻⁵ auMy ⁻¹]
353498	16.52	2.86582	0.04430	0.03658	70.772	-65.349	1.47	31	7.26
353895	16.23	2.87084	0.04589	0.03660	71.224	-65.753	1.48	0	10.99
355083	17.34	2.86750	0.04458	0.03717	70.903	-65.468	1.49	0	12.43
355118	17.02	2.86632	0.04435	0.03673	70.812	-65.384	1.49	0	12.04
355127	16.80	2.86570	0.04427	0.03601	70.779	-65.347	2.73	79	1.71
358354	16.72	2.85929	0.04265	0.03631	70.218	-64.850	1.49	180	-9.84
359840	17.41	2.86720	0.04496	0.03664	70.896	-65.468	1.49	127	-7.72
360906	16.91	2.86651	0.04450	0.03707	70.819	-65.398	1.49	48	6.69
360909	16.82	2.86687	0.04462	0.03715	70.850	-65.427	1.49	69	3.46
363905	17.10	2.86956	0.04534	0.03602	71.124	-65.651	1.49	28	9.75
363995	17.11	2.85981	0.04230	0.03621	70.260	-64.874	1.50	32	9.40
364051	16.79	2.86133	0.04307	0.03648	70.385	-65.001	1.49	115	-4.10
364937	16.93	2.86623	0.04455	0.03704	70.797	-65.381	1.49	0	12.86
366001	16.81	2.86575	0.04451	0.03691	70.759	-65.348	5.88	67	3.67
366971	16.98	2.86432	0.04390	0.03715	70.625	-65.227	1.49	122	-5.68
367544	17.42	2.86625	0.04469	0.03688	70.805	-65.390	1.49	131	-8.49
371188	16.63	2.86038	0.04262	0.03660	70.299	-64.920	1.48	0	9.03
374599	17.09	2.86039	0.04300	0.03717	70.286	-64.927	1.54	156	-10.14
375342	16.85	2.86377	0.04358	0.03636	70.598	-65.188	1.50	74	2.67
375449	17.21	2.86198	0.04327	0.03621	70.449	-65.055	1.49	112	-4.37
375922	16.45	2.86026	0.04282	0.03671	70.287	-64.917	1.50	180	-9.75
376610	15.98	2.86711	0.04458	0.03674	70.882	-65.447	1.49	22	6.10
378764	17.05	2.86162	0.04306	0.03630	70.415	-65.022	1.49	96	-1.16
378817	17.40	2.86746	0.04503	0.03668	70.918	-65.488	1.49	120	-6.45
378866	17.08	2.86799	0.04493	0.03605	70.982	-65.528	1.54	20	10.31
378889	17.21	2.86722	0.04495	0.03706	70.885	-65.464	1.49	127	-7.06
378892	17.02	2.87000	0.04561	0.03654	71.150	-65.685	1.02	25	9.66
379043	17.16	2.86760	0.04480	0.03632	70.939	-65.494	1.49	62	5.33
379071	16.93	2.86399	0.04406	0.03565	70.641	-65.226	1.49	180	-10.73
380470	17.15	2.86204	0.04343	0.03717	70.428	-65.054	1.49	140	-8.70
381469	16.97	2.86649	0.04452	0.03673	70.828	-65.402	1.49	73	2.95
381590	16.81	2.86307	0.04385	0.03732	70.513	-65.138	0.00	152	-8.61
381934	16.70	2.86230	0.04348	0.03700	70.455	-65.075	1.49	134	-6.51
384914	16.48	2.86417	0.04376	0.03558	70.656	-65.230	1.49	61	4.03

Continued on next page

Table 1 – *Continued from previous page*

Number	H	a_P [au]	e_P	$\sin i_P$	g_P " yr ⁻¹	s_P " yr ⁻¹	LCE 10 ⁻⁶ yr ⁻¹	ϵ [deg]	Drift speed [10 ⁻⁵ auMy ⁻¹]
384978	17.27	2.86430	0.04376	0.03627	70.647	-65.230	1.50	63	5.31
386308	16.90	2.86885	0.04554	0.03677	71.042	-65.601	1.60	147	-8.47
387025	16.83	2.86723	0.04468	0.03672	70.894	-65.459	1.75	72	2.93
387694	16.80	2.86675	0.04487	0.03640	70.864	-65.437	1.48	180	-10.08
387700	16.32	2.86437	0.04406	0.03718	70.629	-65.236	1.49	140	-6.00
387971	17.04	2.85980	0.04279	0.03649	70.256	-64.887	1.51	131	-7.19
389182	16.70	2.85873	0.04245	0.03718	70.145	-64.795	1.49	180	-12.90
389186	17.03	2.85796	0.04183	0.03624	70.104	-64.732	1.38	0	10.90

REFERENCES

- Bottke, W. F., Vokrouhlický, D., Rubincam, D.P., Brož, M. 2002, in Asteroids III, ed. W. F. Bottke et al. (Tucson: University of Arizona Press), 395
- Bottke, W. F., Vokrouhlický, D., Rubincam, D. P., & Nesvorný, D. 2006, *Annu. Rev. Earth Planet. Sci.*, 34, 157
- Bottke, W. F., Vokrouhlický, D., Walsh, K. J., et al. 2015, *Icarus*, 247, 191
- Brož, M. 1999, Master Thesis, Charles University, Prague, Czech Republic
- Brož, M., Morbidelli, A., Bottke, W. F., et al. 2013, *A&A*, 551, A117
- Bus, S. J., & Binzel, R. P. 2002a, *Icarus*, 158, 106
- Bus, S. J., & Binzel, R. P. 2002b, *Icarus*, 158, 146
- Čapek, D., & Vokrouhlický, D. 2004, *Icarus*, 172, 526
- Carruba, V. Huaman, M. E., Domingos, R. C., & Roig, F. 2013, *A&A*, 550, A85
- Carruba, V., Nesvorný, D., Aljbaae, S., & Huaman, M. E. 2015, *MNRAS*, 451, 4763
- Delbò, M., Dell’Oro, A., Harris, A. W., Mottola, S., & Mueller, M. 2007, *Icarus*, 190, 236
- DeMeo, F. E., & Carry, B. 2013, *Icarus*, 226, 723

- Ďurech, J., Hanuš, J., Oszkiewicz, D., & Vančo, R. 2016, *A&A*, 587, A48
- Giblin, I., Martelli, G., Farinella, P., et al. 1998, *Icarus*, 134, 77
- Golubov, O., & Krugly, Y. N. 2010, *ApJLett*, 752, L11.
- Hanuš, J., Ďurech, J., Brož, M., et al. 2011, *A&A*, 530, 134
- Harris, A. W., Mueller, M., Lisse, C. M., & Cheng, A. F. 2009, *Icarus*, 199, 86
- Ivezić, Ž., Tabachnik, S., Rafikov, R., et al. 2001, *AJ*, 122, 2749
- Lazzaro, D., Angeli, C. A., Carvano, J. M., et al. 2004, *Icarus*, 172, 179
- Levison, H. F., & Duncan, M. J. 1994, *Icarus*, 108, 18
- Masiero, J. R., Mainzer, A. K., Grav, T., Bauer, J. M., & Jedicke, R. 2012, *ApJ*, 759, 14
- Mignard, F., Cellino, A., Muinonen, K., et al. 2007, *EM&P*, 101, 97
- Milani, A., & Knežević, Z. 1994, *Icarus*, 107, 219
- Molnar, L. A., & Haegert, M. J. 2009. AAS/Division for Planetary Sciences Meeting Abstracts #41 41, #27.05
- Murray, C. D., & Dermott, S. F. 1999, *Solar System Dynamics* (Cambridge University Press, Cambridge)
- Nesvorný, D., Bottke, W. F., Dones, L., & Levison, H. F. 2002, *Nature*, 417, 720
- Nesvorný, D., & Bottke, W. F. 2004, *Icarus*, 170, 324
- Nesvorný, D., Enke, B. L., Bottke, W. F., et al. 2006, *Icarus*, 183, 296
- Nesvorný, D., Brož, M., & Carruba, V. 2015, in *Asteroids IV*, ed. P. Michel et al. (Tucson: University of Arizona Press), 297
- Novaković, B., Hsieh, H. H., & Cellino, A. 2012, *MNRAS*, 424, 1432
- Novaković, B., Clara, M., Tsirvoulis, G., & Knežević, Z. 2015, *ApJ*, 807, L5
- Pravec, P., Harris, A. W., & Michalowski, T. 2002, in *Asteroids III*, ed. W. F. Bottke et al. (Tucson: University of Arizona Press), 113
- Pravec, P., Harris, A. W., Vokrouhlický, D., et al. 2008, *Icarus*, 197, 497

- Press, V. H., Teukolsky, S. A., Vetterlink, W. T., & Flannery, B. P. 2001, *Numerical Recipes in Fortran 77* (Cambridge University Press, Cambridge)
- Rayman, M. D., *Dawn Journal*, May 28, 2015
- Rozitis, B., & Green, S. F. 2012, *MNRAS*, 423, 367
- Rubincam, D. P. 2000, *Icarus*, 148, 2
- Šidlichovský, & M., Nesvorný, D. 1997, *Cel. Mech. Dynam. Astron.*, 65, 137
- Slivan, S. M., & Molnar, L. A. 2012, *Icarus*, 220, 1097
- Tholen, D. J. 1989, in *Asteroids II*, ed. R. P. Binzel et al. (Tucson: University of Arizona Press), 1139
- Vokrouhlický, D. 1999, *A&A*, 334, 362
- Vokrouhlický, D., Nesvorný, D., & Bottke, W. F. 2003, *Nature*, 425, 147
- Vokrouhlický, D., Brož, M., Bottke, W. F., Nesvorný, D., & Morbidelli, A. 2006a, *Icarus*, 182, 118
- Vokrouhlický, D., Nesvorný, D., & Bottke, W. F. 2006b, *Icarus*, 184, 1
- Vokrouhlický, D., Bottke, W. F., Chesley, S. R., Scheeres, D. J., & Statler, T. S. 2015, in *Asteroids IV*, ed. P. Michel et al. (Tucson: University of Arizona Press), 509
- Xu, S., Binzel, R. P., Burbine, T. H., & Bus, S. J. 1995, *Icarus*, 115, 1
- Zellner, B., Tholen, D. J., & Tedesco, E. F. 1985, *Icarus*, 61, 355

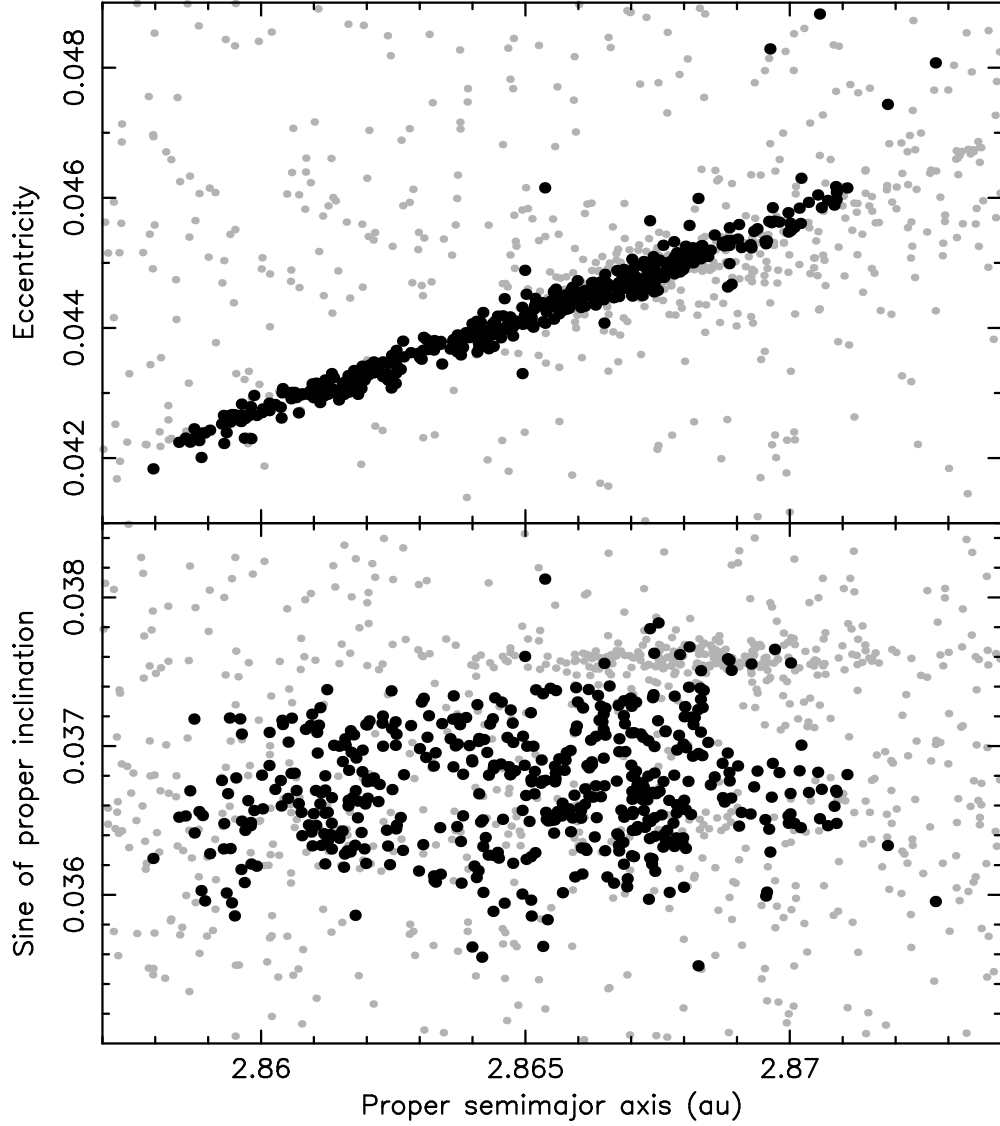


Fig. 1.— A (a, e) (top panel) and $(a, \sin i)$ (bottom panel) projection of members of the Karin cluster that satisfy the selection criteria discussed in Sect. 3 (480 members, full black dots), and of asteroids in the local background (full gray dots). The alignment of background gray objects seen for $\sin i \simeq 0.0375$ is the Koronis(2) family (Molnar & Haegert 2009).

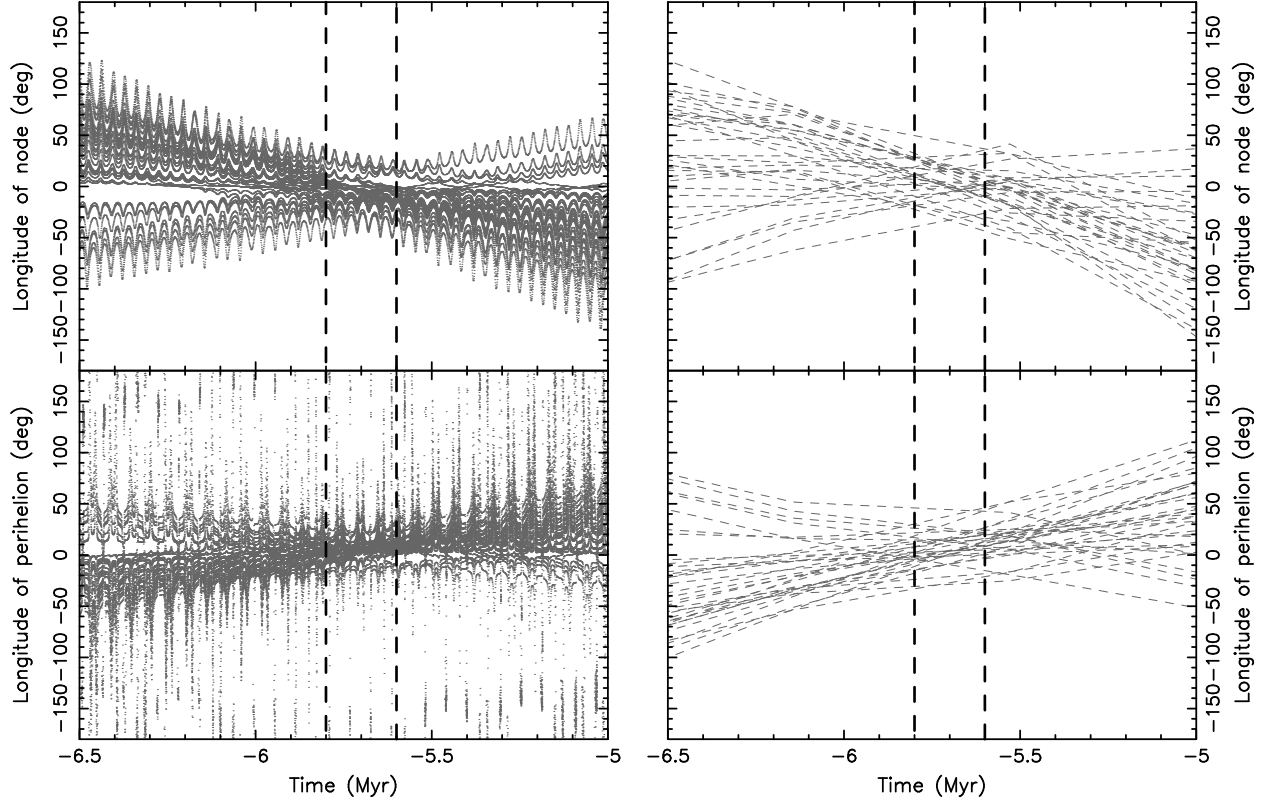


Fig. 2.— Past evolution of the osculating (left panel) and mean (right panel) Ω and ϖ angles for 34 large members of the Karin cluster. The vertical dashed lines delimit the time interval between -5.6 and -5.8 My. The mean perihelion and nodal longitudes were obtained using the Frequency Modified Fourier Transform (FMFT) method of Šidlichovský & Nesvorný (1997). The convergence of angles of all these large members of the Karin cluster were originally reported in Nesvorný & Bottke (2004).

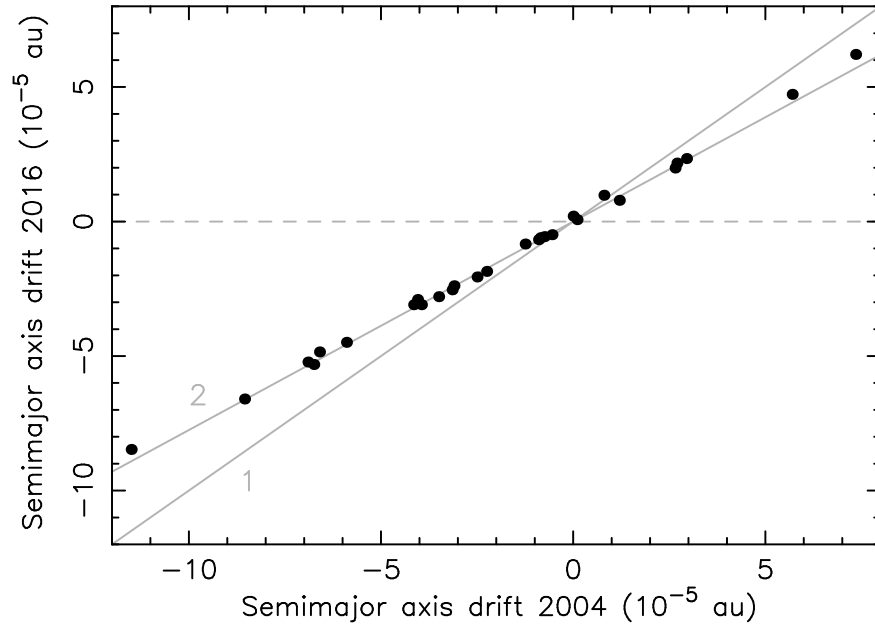


Fig. 3.— Correlation between the drifts found in Nesvorný & Bottke (2004) and those obtained from the present analysis. The gray line 1 has a slope 1; the gray line 2 has a shallower slope 0.8, implying the values obtained in this work are about 20% smaller (see the text for explanation).

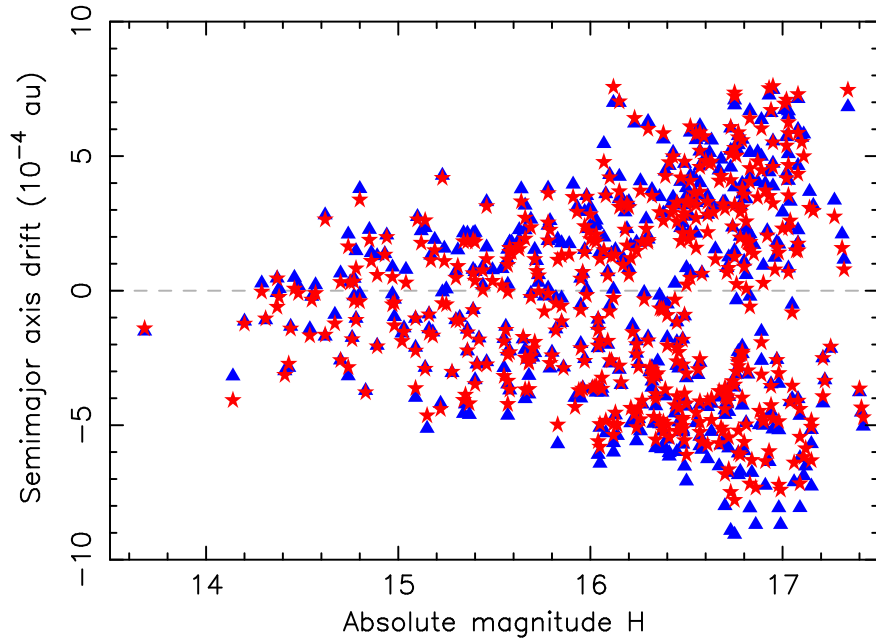


Fig. 4.— Semi-major axis drift Δa for 480 Karin cluster members that we inferred from the convergence of secular angles at $\tau = 5.746$ My. The blue triangles and the red stars denote the Δa values computed over the estimated family age from $\Delta\Omega$ and $\Delta\varpi$, respectively. There is a good consistency between the two determinations.

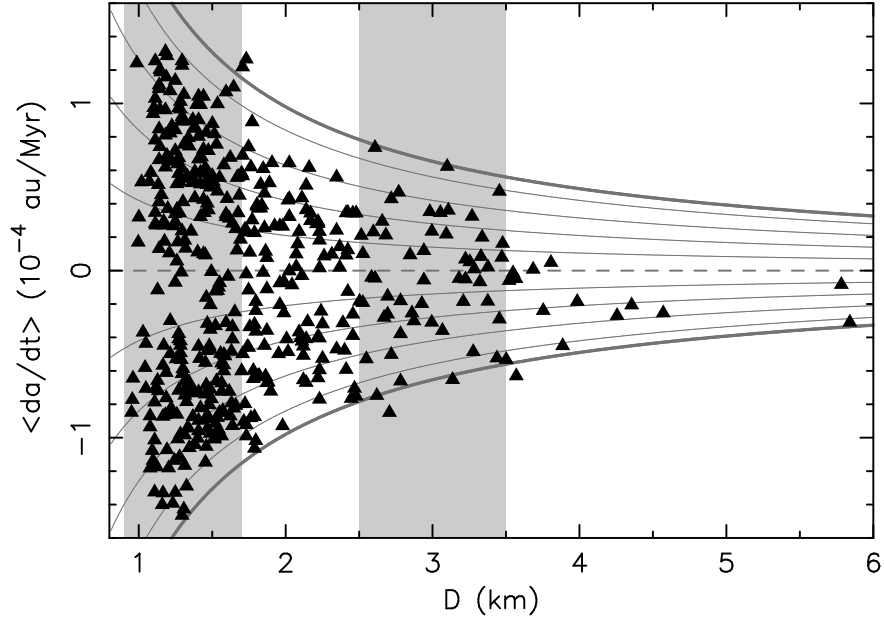


Fig. 5.— The effective drift rate $\langle da/dt \rangle$ of the Karin cluster members (ordinate) vs their diameter D (abscissa). The gray lines are isolines of $\langle da/dt \rangle \propto 1/D$. If we choose $D = 1.4$ km as reference value, the thin lines correspond to $\langle da/dt \rangle$ values of $\pm(3, 6, 9, 12) \times 10^{-5}$ au/My. The thick gray lines, approximately enclosing all data-points, correspond to $\langle da/dt \rangle = \pm 1.4 \times 10^{-4}$ au/My for $D = 1.4$ km. The two size ranges, shown by the light gray rectangles, are $D = 0.9 - 1.7$ km (denoted I1) and $D = 2.5 - 3.5$ km (denoted I2). The interval I1 contains 280 data-points, while I2 contains 55 data-points. The distribution of drift rates in I1 is clearly bimodal with only a few bodies with $\langle da/dt \rangle \simeq 0$. The drift rates in I2 are roughly evenly distributed.

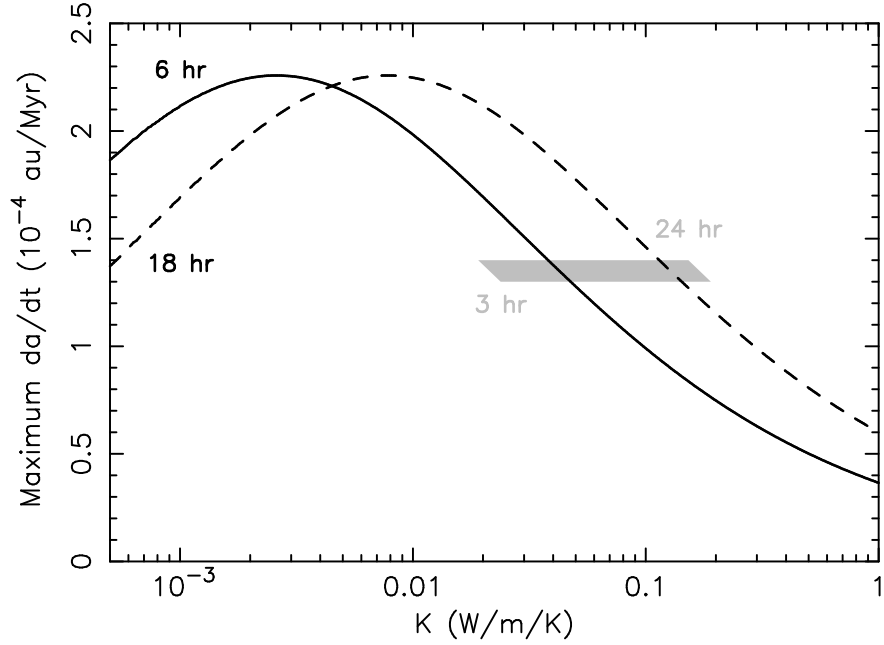


Fig. 6.— Theoretical value of the diurnal Yarkovsky drift rate da/dt at zero obliquity (Eq. 6) as a function of the surface thermal conductivity for $D = 1.4$ km. We assumed Bond albedo $A = 0.1$, thermal emissivity $\epsilon = 0.9$, bulk density $\rho_b = 2.5$ g cm $^{-3}$, surface density $\rho_s = 2$ g cm $^{-3}$ and heat capacity $C = 680$ J kg $^{-1}$ K $^{-1}$. The rates were computed for two values of the rotation period, $P = 6$ hr (solid line) and $P = 18$ hr (dashed line). Because da/dt is a function of K/P , the results can be easily rescaled to other periods. The gray trapezoid highlights $da/dt = (1.3 - 1.4) \times 10^{-4}$ au My $^{-1}$, which is roughly the range of the maximum drift rates in Fig. 5.

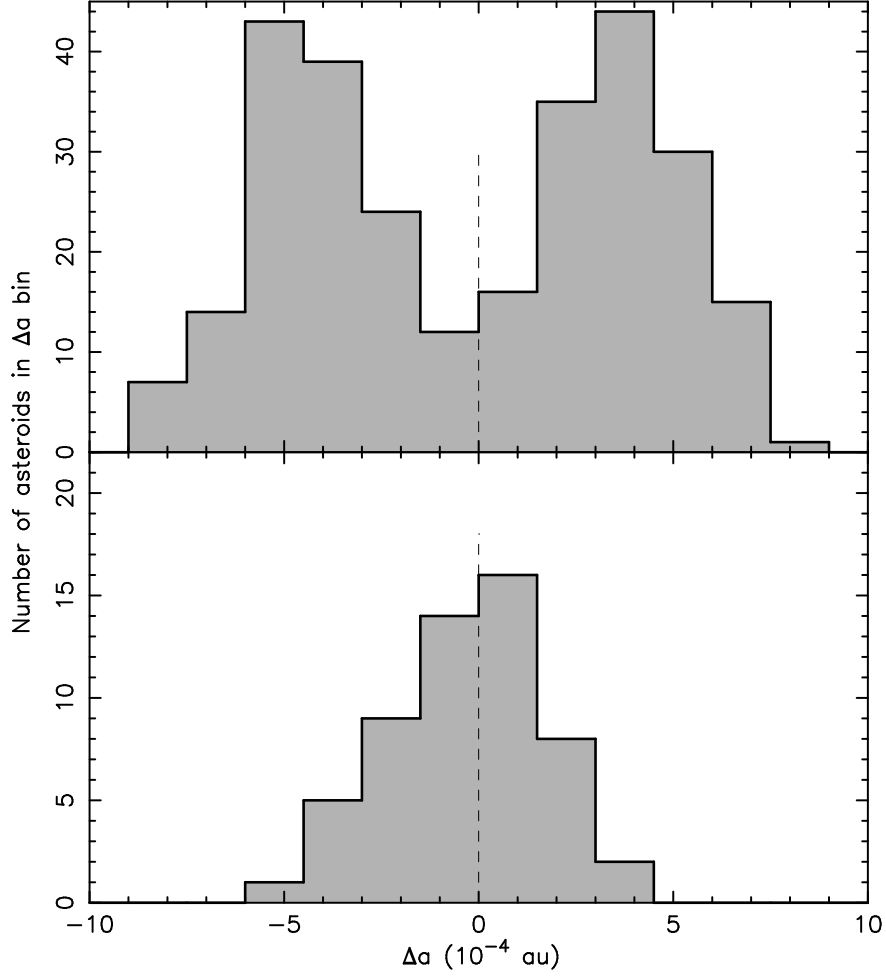


Fig. 7.— The distribution of Δa values in the intervals I1 (top) and I2 (bottom). Here we use a bin size of 1.5×10^{-4} au. Top: The sample contains 280 bodies with equally populated negative and positive values (139 vs. 141). The distribution is clearly bimodal. The median negative and positive values are $\simeq -4.3 \times 10^{-4}$ au and $\simeq 3.4 \times 10^{-4}$ au, respectively. Bottom: The sample contains 55 bodies. There is no statistically significant difference between the number of negative and positive values (29 vs 26). Here the distribution is peaked at the origin.

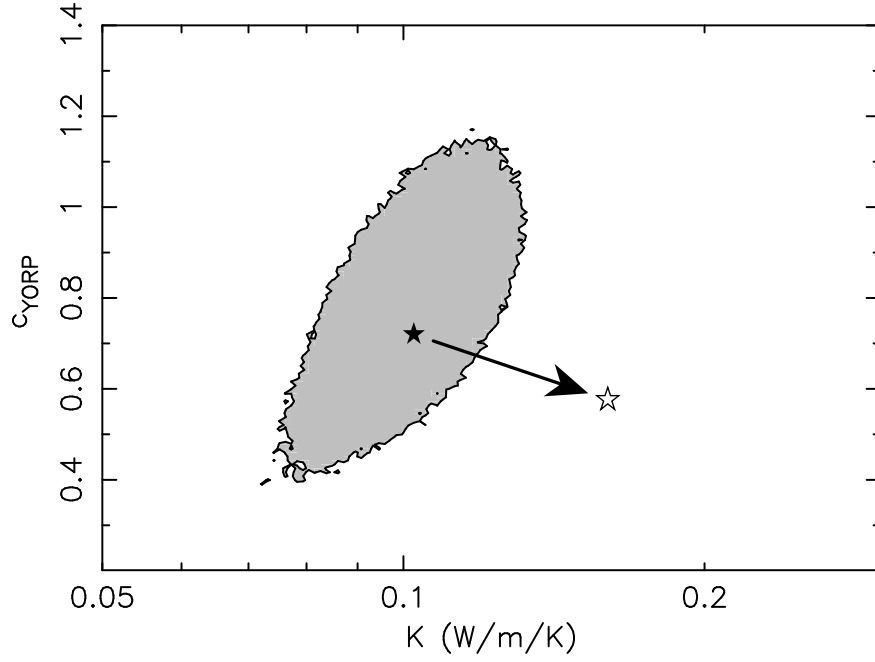


Fig. 8.— The confidence interval defined as $\chi^2 < N$ with $N = 12$ (gray zone). The best fit solution is denoted by the black star. Here we fixed $\delta_{\text{YORP}} = 0.4$ and varied the surface conductivity K (abscissa) and the c_{YORP} parameter. The bulk density was assumed to be 2.5 g/cm^3 . If $\rho_b = 2 \text{ g/cm}^3$ instead, the best fit solution would move as indicated by the arrow, and the confidence region would shift as well.

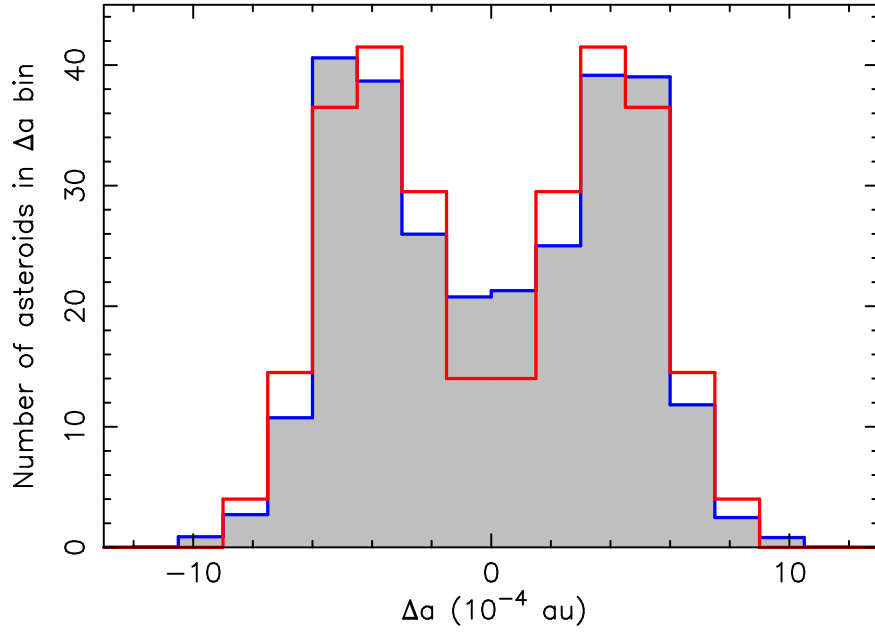


Fig. 9.— The best fit solution for $\delta_{\text{YORP}} = 0.4$, $K^* = 0.1 \text{ W m}^{-1} \text{ K}^{-1}$ and $c_{\text{YORP}}^* = 0.72$ (the gray histogram and blue line). The distribution of drift values inferred from the convergence criterion is shown by the red histogram.

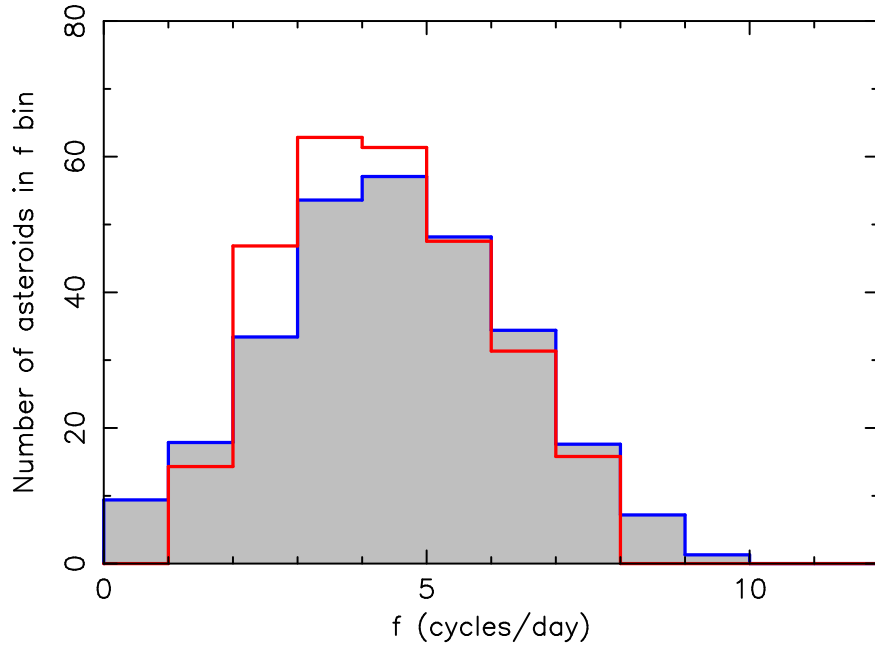


Fig. 10.— Illustration of the YORP effect on the rotation frequencies in the best fit from Fig. 9. The abscissa shows the rotation frequency $f = \omega/2\pi$ in cycles per day. The red histogram was the assumed initial distribution of the rotation frequencies. The gray histogram shows the final distribution at $\tau = 5.746$ My.

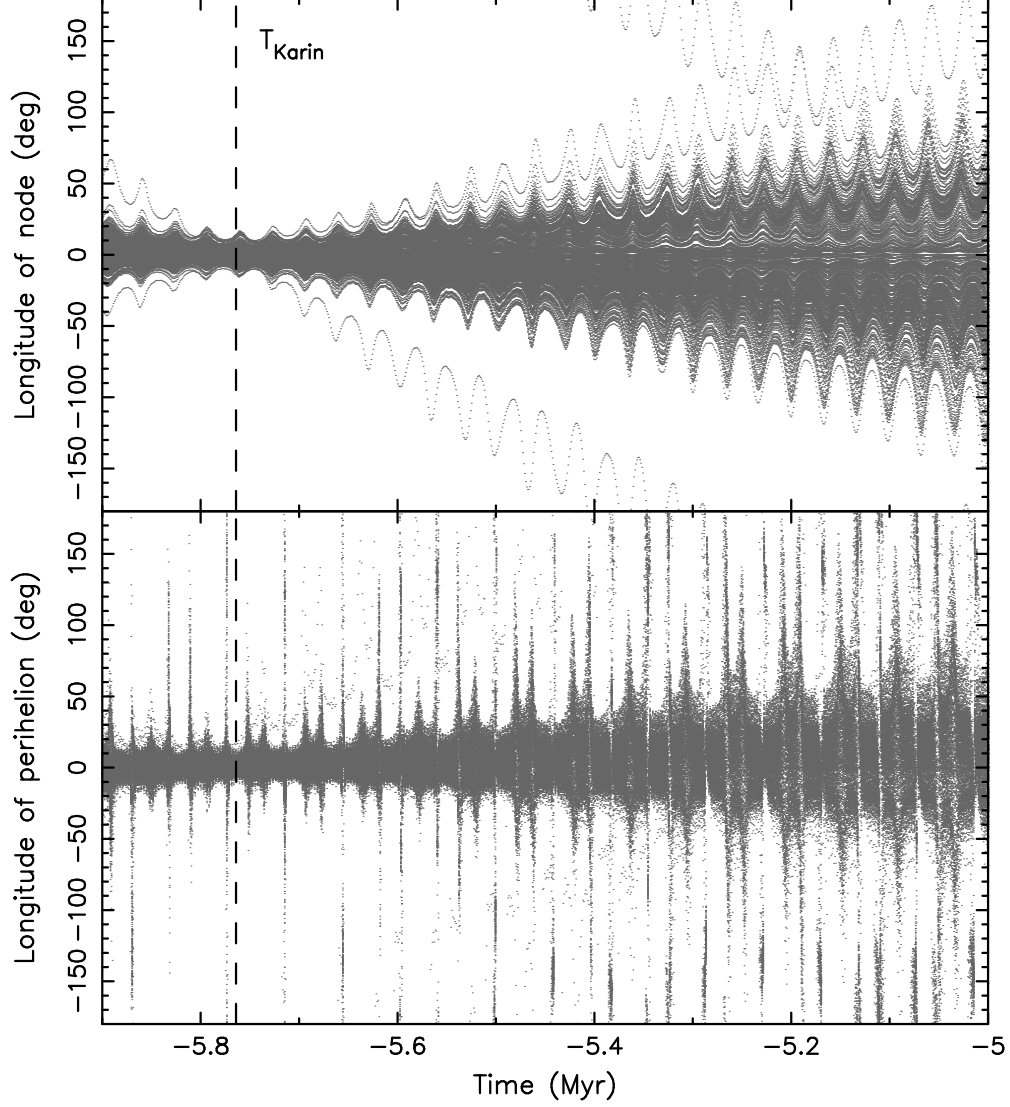


Fig. 11.— The past orbital histories of 322 members of the Karin cluster: nodal longitude (top) and perihelion longitude (bottom). The values of these angles are given here relative to (832) Karin. Unlike in Fig. 2, here we accounted for the Yarkovsky effect explicitly in the integration. As a result, the convergence at $\tau = -5.764$ Myr has significantly improved.

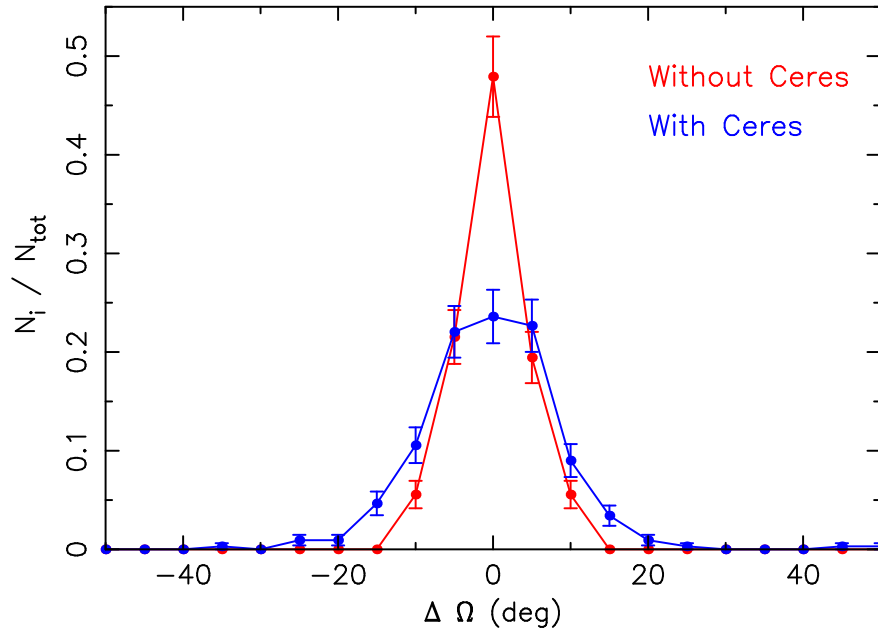


Fig. 12.— The distribution of Ω values at $\tau = -5.764$ My for the cases without Ceres (red line) and with Ceres (blue line). The error bars are assumed to be proportional to the square root of the number of objects in each bin.

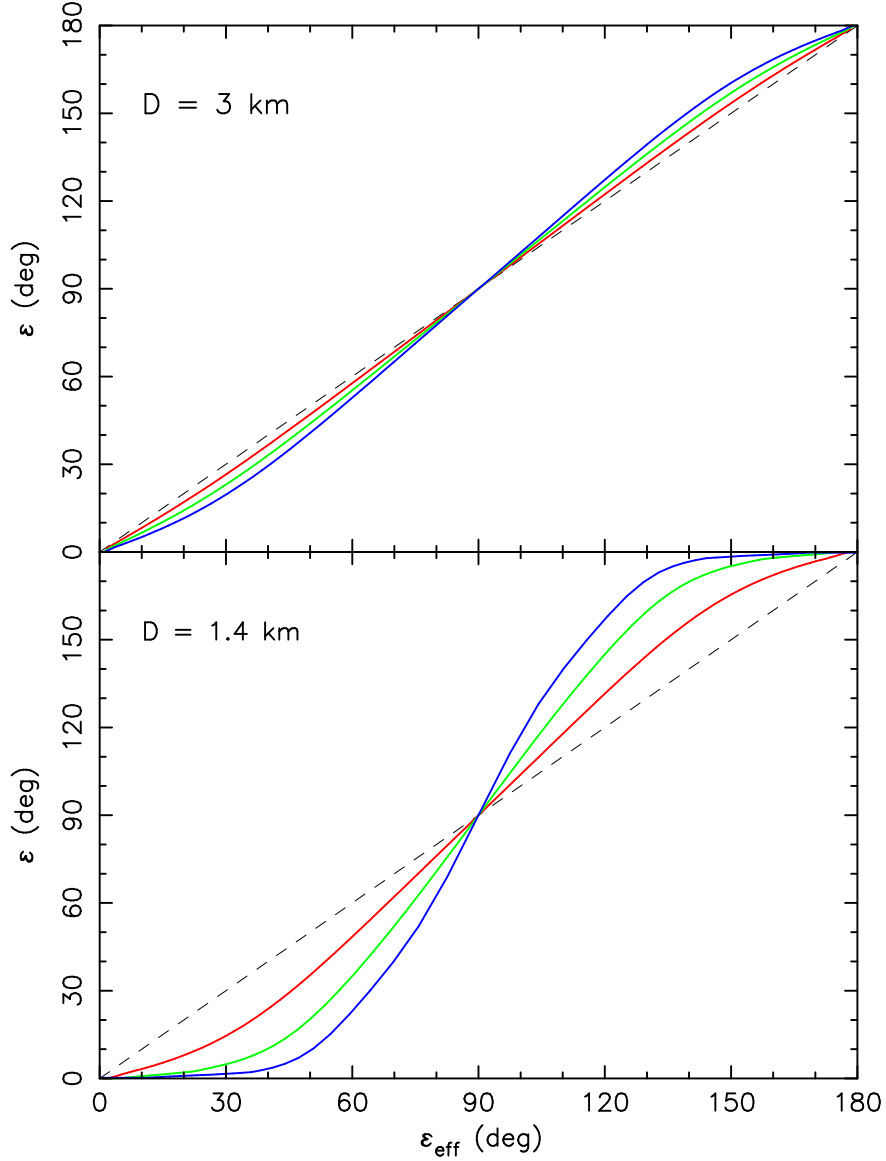


Fig. 13.— Relation between the effective obliquity ε_{eff} (column 9 of Table 1) and the current obliquity ε (ordinate) of the simulated bodies in the Karin family. The top panel is for $D = 3 \text{ km}$ members, a representative size in the interval I2, while the bottom panel is for $D = 1.4 \text{ km}$ members (representative for I1). The three curves in each of the panels were obtained for different rotation periods: 4 hr (red), 8 hr (green), and 12 hr (blue). For a larger asteroid size in the top panel, both obliquity values nearly coincide. For a smaller size, the effective obliquity ε_{eff} can be slightly larger (if $\varepsilon_{\text{eff}} < 90^\circ$) or smaller (if $\varepsilon_{\text{eff}} > 90^\circ$) than the current value of ε , especially if the rotation rate is slow.